KERNFORSCHUNGSZENTRUM

KARLSRUHE

The PHAETON 2 Computer Code for Analysing Accidents in a 1000 MWe Helium Cooled Fast Reactor

D. Wilhelm

KERNFORSCHUNGSZENTRUM KARLSRUHE

KFK 2561

Institut für Neutronenphysik und Reaktortechnik
Projekt Schneller Brüter

The PHAETON2 computer code for analysing accidents in a 1000 MWe
helium cooled fast reactor

D. Wilhelm
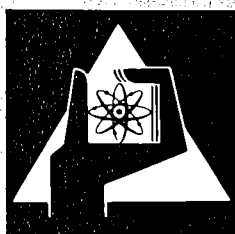
Gesellschaft für Kernforschung m.b.H., Karlsruhe

Abstract

The PHAETON2 computer code is based upon the solution of the one-dimensional fluid dynamics equations in order to calculate the transient behaviour of Gas Cooled Fast Reactors (GCFR). The type of accidents that are of major interest for the safety of GCFRs imposes to the code to calculate a few minutes of the problem time during which transient effects are dominant with time constants longer than a second.

The code model and methods of solution are described and a set of depressurization and flow-coast-down accidents is discussed for a 1000 MWe GCFR with secondary steam loops.

Das Rechenprogramm PHAETON2 - Unfallanalyse eines 1000 MWe Heliumgekühlten Schnellen Brutreaktors

Zusammenfassung

Das Rechenprogramm PHAETON2 basiert auf der Lösung der eindimensionalen fluiddynamischen Gleichungen zur Berechnung des instationären Verhaltens von Gasgekühlten Schnellen Brutreaktoren (GCFR). Die für die Sicherheit der GCFRs wichtigsten Unfallarten bestimmen, daß das Rechenprogramm vor allem Probleme mit Zeitkonstanten von mehr als einer Sekunde über wenige Minuten zu verfolgen hat.

Das Modell und die Lösungsmethoden des Rechenprogramms werden beschrieben, und eine Reihe von Druckverlust- und Durchsatzverlustunfällen eines 1000 MWe - Reaktors mit sekundärem Dampfkreislauf wird diskutiert.

Contents

1. Introduction

Safety aspects of GCFRs are closely connected to the special
features of the primary loops such as high helium pressure
inside a prestressed concrete reactor vessel (PCRV), vented
fuel pins, artificial roughness of the cladding surface for
better heat transfer, and redundant helium circulators. As the
reactivity effects of the coolant are small, attention has to
be paid mainly to maintaining sufficient heat removal from the
core. If reactivity supplies from outside, like malfunctioning
of control rods, which could impose steep reactivity ramps, are
neglected all major accidents typical of the GCFR lead to rather
slow transients. This is a result of great constructional efforts.
The PCRV, for example, is highly redundant and all penetrations
which could fail are made as small as possible. Because of these
slow transients and since helium is a perfect gas, computer codes
to simulate accidents can profit from many simplifications. One
of the conservative GCFR-designs is based upon the use of
secondary steam loops with a huge steam turbine connected to
the electrical generator, as also used in LMFBRs. Partitioning
into a primary helium loop and a secondary steam loop, both
connected by a heat exchanger, and use of cylindrical fuel
pins clustered into subassemblies are basic requirements for oper-
ating the PHAETON2 computer code. In this report only one special
1000 MWe GCFR-design with a hanging core is discussed.

Zum Druck am: 19.12.1977

2. The object

2.1 Description of the GCFR with secondary steam cycle

Fig. 1 shows a cross-sectional view of the PCRV of the 1000 MWe
reactor proposed by Kraftwerk Union, Erlangen, Federal Republic
of Germany /1/ /2/.
A central cavity contains the reactor core with the inlet plenum
above and the huge exit plenum below it.
In 8 circumferential cavities represented on the left-hand side
of the cross section the helium-water heat exchangers are
located with the helium circulators directly connected to
single-stage steam turbines at the upper end.
The right-hand side of the cross section shows one of 4 auxiliary
heat exchangers and an auxiliary circulator driven by an electric
motor. The primary loops contain helium at high pressure. Helium
flows from the reactor outlet plenum to the resuperheater at the
lower end of the cavity. From there it is directed to the upper
end of the steam generator through a central tube. It flows
downwards through the steam generator and turns upwards again to
enter the circulator inlet plenum at the upper end of the cavity.
The circulator exit plenum is directly connected to the reactor
inlet plenum.
In the secondary loops the water is pressurized by feedwater
pumps and carried to the steam generator. Dry steam then enters
the helium circulator and is heated up afterwards in a resuper-
heater. From there it leaves the PCRV for the main steam turbine
which drives the electrical generator.

Fig. 2 shows a model of the 1000 MWe reactor as used by the
PHAETON2 computer code. It can be seen that the geometrical
build-up is similar in figs. 1 and 2. Some of the features of
fig. 2 are described later-on when dealing with the code model.

-

2.2 Some special features of the gas loops

Both primary helium loops and secondary steam loops are closely connected by the heat exchangers and the turbo-machines (see fig.2). As all of the steam is directed through the circulator turbine, the mass flows in the primary and secondary cycles are nearly proportional in most cases. The small inertia of the shaft allows to change its speed quickly.
As the whole energy generated in the core is transmitted to the secondary loop by the huge heat exchangers, there is always a close thermal linkage between both cycles. In the primary cycle the main pressure drops occur in the core characterized by high energy densities. Most plant controls are only effective on the secondary loop, which, consequently, changes the conditions in the primary loop. Feed water pumps are regulated by their speed; valves can be closed in front of the circulator and main turbines. The main turbine can be by-passed, the secondary loop then being coupled to a constant pressure of the condenser system.

2.3 The main features of the reactor core

The hanging core is made up of hexagonal subassemblies; the helium passes through them in the opposed direction to natural convection. Each subassembly contains bundles of pins which are radially fixed by spacers.
The vented pins are surrounded by a steel cladding parts of which are roughened by transversal ribs.

Reactivity coefficients are negative for Doppler, axial, and radial expansion effects. The coolant density coefficient is negative, i.e. the reactivity increases with decreasing helium density. Considering the neutron density, the fast core is strongly coupled so that point kinetics is sufficient for sub-prompcritical conditions. Due to different breeding ratios the core and the blanket generate different amounts of shut-down heat.

The principal data of the GCFR considered are shown in fig. 13. It is a 1000 MWe reactor built by Kraftwerk Union, which has been chosen for transient analyses by the PHAETON2 computer code. Some typical results are published in this paper.

3. The model and the main equations

3.1. The aim of the model describing the GCFR

The principal item of the GCFR-model is the description of
the transient behaviour of the fluid and the adjacent
structures. The complicated arrangements of the cooling
circuits should be fully taken into account whereas changes
of geometry with time should be neglected when considering the
melting of the clad.
Any solution will have to allow for implementation of a technical
correlation of heat transfer and pressure drop which can be
calculated with mixed mean fluid properties.
Therefore, a one-dimensional form of the conservation equations
seems to be most appropriate as two-dimensional calculations in
the core will take too much time for computer calculations.
Thus, important features of the rest of the loop have not to be
neglected in order to stay inside computer time limits. The
biggest drawback inside the reactor core is that propagation
effects and radial exchanges inside a subassembly cannot be
calculated. The core and blanket should be represented by a
number of pins that stand for the average characteristic of the
location being modelled. As in a pin the energy transport is
much bigger in the radial than in the axial direction, a
one-dimensional form of the Fourier-equation is possible on the
assumption of symmetry with respect to the pin axis.
The model is now specified to fit the needs of the following
equations: one-dimensional unsteady conservation equations
for mass, momentum and energy for the fluid,
one-dimensional unsteady heat-conduction equation
in the adjacent structure,
quasi-steady energy and momentum transfer between
fluid and wall
zero-dimensional equation for the energy release
in the core.

3.2. The one-dimensional fluid dynamics equations

The conservation equations for mass, momentum, and energy are given in Euler-coordinates for a tube with the cross-sectional area F and the axial coordinate x. The one-dimensional form can be chosen if all fluid properties are uniform with respect to F and if the fluid is only moving in the x-direction. This leads to the mass equation

$$\frac{\partial}{\partial t} (\rho F) + \frac{\partial}{\partial x} (\rho\, w\, F) = 0 \tag{1}$$

with t being the time, ρ the density, and w the velocity in the x-direction.

In the momentum equation, K_v stands for the friction force per fluid volume acting on the adjacent wall; g is the gravitational acceleration; γ the angle that the tube forms with the horizon; and p the pressure:

$$\frac{\partial}{\partial t} (\rho w F) + \frac{\partial}{\partial x} (pF + \rho w^2 F) + g\rho F \sin\gamma + K_v\, F - p\frac{\partial F}{\partial x} = 0 \tag{2}$$

The first term and the second part of the second term describe the influences of the local and convective acceleration, respectively; the first part of the second term describes the influence of the pressure acting on the cross sectional area. The following terms are defined by the gravity force, the friction force, and the force acting on the projection of the peripheral wall on the cross sectional area. The friction forces are given by technical correlations formed by algebraic functions.

In the energy equation, u is the internal energy of the fluid, i is the enthalpy, and q_v is the power per fluid volume that is coming in from outside:

$$\frac{\partial}{\partial t}\left((u + \frac{w^2}{2})\rho F\right) + \frac{\partial}{\partial x}\left((i + \frac{w^2}{2})\rho w F\right) + p\frac{\partial F}{\partial t} + g\rho w F \sin\gamma - q_v F = 0 \tag{3}$$

The first and second terms describe the changes of energies stored in the fluid, the third term gives the change of energy due to a time-dependent variation of the cross-sectional area, i.e. for a rigid system. The fourth term describes the change of energy due to gravity and the last term that caused by an energy source, which will be given by an algebraic function.

The friction force K_v is substituted in chapter 4.7. by terms depending on the Weisbach friction factor λ and the drag coefficient ζ. Both parameters are obtained from steady-state experiments and can be used also in transient calculations of a helium-loop; see /22/.

When substituting q_v (see chapter 4.8.), correlations are found with the heat-transfer coefficient as a main parameter. This is a result of steady-state measurements and can be used for transient calculations as well/22/. When neglecting the disassembly phase, the third term of the energy equation with $\frac{\partial F}{\partial t}$ and the equivalent in the mass equation can be cancelled. In the following discussion about the conservation equations we distinguish between the description of the primary loop with an ideal gas and the secondary loop with steam.

3.3. The fluid dynamics equations for the helium loops

Rewriting the set of equations (1) (2) while neglecting that the cross-sectional areas will be constant with respect to time (pulsating wall, disassembly phase) gives

$$\frac{\partial \rho}{\partial t} = - \frac{1}{F} \frac{\partial m}{\partial x} \tag{5}$$

$$\frac{\partial m}{\partial t} = -F \frac{\partial p}{\partial x} + \frac{m^2}{\rho^2 F^2} \frac{\partial}{\partial x} (\rho F) - \frac{2m}{\rho F} \frac{\partial m}{\partial x} - g\rho F \sin\gamma - K_v F \tag{6}$$

Without the terms of kinetic energy, gravity, and pulsating wall the energy equation (3) is reduced to

$$F\frac{\partial}{\partial t} (u\rho) + \frac{\partial}{\partial x} (i\rho wF) - q_v F = 0 \qquad (7)$$

If we define the power per volume generated by the heat flux through the wall by

$$q_v = \frac{T_{wall} - T}{F R_w} \qquad (11)$$

with R_w being the thermal resistance between fluid and adjacent wall, the energy equation becomes

$$F\frac{\partial}{\partial t} (c_v T\rho) + \frac{\partial}{\partial x} (c_p T m) - \frac{T_{wall} - T}{R_w} = 0 \qquad (12)$$

The simplifications in the energy equation anticipate the existence of a method which will separate the energy equation from the rest of the whole set (non-simultaneous solution).

3.4. Non-simultaneous solution of the one-dimensional fluid dynamics equations

The main feature of the solution of the conservation equations in the PHAETON2 computer code is the separation of the equations to achieve a flexible, problem-oriented model of the loops.

By discretising the length increments of the one-dimensional equations, the non-simultaneous solution will already become obvious if two nodal systems are established. Each of these systems describes the same loop model but it forms its own length increments. The aim of forming these increments is to arrange a high number of nodes where the independent variables change rapidly with the length. Solutions for the independent variables of one nodal system are transformed into the geometry of the other nodal system and vice versa.

By discretising the time increments it is possible to use
different methods of integration step sizes in each of the
nodel system according to the time constants of the governing
equations. The link between both nodel systems will again be
a transformation the quality of which has an influence on the
stability and accuracy of the solutions.

3.5 The fluid dynamics equations for the steam loops

In the steam-loop calculations many simplifications are
possible because of the negligible influence they exert on the
solutions of the primary loops. The secondary loops represent,
so to speak, boundary conditions for the primary loops and are
characterized by control systems which are not known in detail
by now. Thus, the user of the code specifies himself the control
parameters in a rather rough manner. This leads to the
requirement of calculating only major effects in the secondary
loop.

Now the conservation equation can be simplified by first
rewriting equation (1):

$$\frac{\partial \rho}{\partial t} + \frac{1}{F} \frac{\partial m}{\partial x} = 0 \tag{13}$$

The momentum equation is reduced to:

$$\frac{\partial m}{\partial t} + \frac{\partial}{\partial x} (pF) + K_v F = 0 \tag{14}$$

if the influence of fluid inertia, of gravity, and of the
change of the cross-sectional area with x is neglected. In
the energy equation, the terms of kinetic energy and gravity
are cancelled:

$$\frac{\partial}{\partial t} (u\rho F) + \frac{\partial}{\partial x} (i\rho w F) - q_v F = 0 \tag{15}$$

The internal energy and enthalpy are linked by

$$i = u + \frac{p}{\rho} \qquad (16)$$

The pressure is obtained by using the equations of state

$$p = p(u,\rho) \qquad (17)$$

These equations are given in the form of data tables which can be used by interpolation routines.

3.6 The choice of the finite elements of the helium loops

The places of high energy exchange, i.e. great changes in helium temperature with axial length, are the reactor core and the helium-water heat exchangers. The nodel system for the solution of the energy equation should arrange a high number of nodes in these areas.
The places of high pressure differences are the reactor core, the helium-water heat exchangers, and the helium circulator. On the other hand, contructional items lead to the formation of a number of big cavities that lie between places of high pressure differences. The nodel system for the solution of the mass and momentum equations should form plena at their true location in the loops and connect them with links where helium mass flows due to the pressure differences of the adjacent plena.
Fig.4 shows a single primary loop model with two plena and three links representing the first nodal system. Now the links are defined to be lines of uniform pressure and density. The momentum equation will be integrated along the links. To allow for compressibility of the fluid in the plena, a simple form of the energy equation must be added to the mass equation. Both equations will be given in a space-integral form since the zero-dimensional plena represent cavities of considerable expansion.

The momentum equation will take into account natural convection. Therefore, it will be appropriate to form links connecting plena of big differences in geodetical heights. The second nodal system in fig.4 is established along the links to solve the energy equation there. Thus, each line is subdived into an arbitrary number of finite elements inside which the temperatures of the helium will be calculated, thus allowing a finite transportation time of the fluid while passing through a finite element. Only here heat exchange will take place while the walls of the plena are supposed to be adiabatic.

A simple transformation method is used to connect both nodal systems.

In each link the inlet temperature is calculated by the simplified energy equation of the first nodal system while the inlet temperatures to the plena are results of the second nodal system. Along the links a linear variation of pressure is assumed with the boundary pressures equal to those of the adjacent plenums. According to the definition above, helium mass flows are uniform along a link.

4. The complementary equations

4.1 The equations describing the energy balance in a link

Along the links the energy equation is solved for helium passing through a tube with the temperatures of the adjacent walls as boundary conditions. These temperatures are solutions of a set of one-dimensional heat conduction equations in the structure material of the wall.

Taking r as the radial distance, a as the thermal diffusivity, q_v as the power per volume inside the wall, c as the specific heat capacity, ρ as the density, the basic heat conduction equation is

$$\frac{\partial T}{\partial t} = a\frac{1}{r}\frac{\partial}{\partial r}\left(r\frac{\partial T}{\partial t}\right) + \frac{q_v}{\rho c} \tag{18}$$

ρ and c are supposed to be independent of r.

Without considerable generation of energy in the structure material (i.e. outside U/Pu-O$_2$-pellets) q_v is set zero, otherwise it is calculated following chapter 4.3. In equation (18) the cylindrical coordinates have been reduced to only one because of symmetry and neglection of axial heat conduction. Along the links the mass flow is constant, and the fluid is incompressible (ρ = constant). By using the ideal gas law

$$T = \frac{p}{\rho R} \tag{19}$$

and the correlation

$$c_v = c_p - \frac{p}{\rho T} \tag{20}$$

with R, c_p and c_v being constants, equation (12) can be written

$$\frac{\partial T}{\partial t} + w\frac{\partial T}{\partial x} = \frac{T_{wall} - T}{R_w \rho c_p F} + \frac{1}{\rho c_p}\frac{\partial p}{\partial t} \tag{21}$$

At this point we remember that the nodal system solving the mass and momentum equations takes into account natural convection.

4.2 The equations describing the hydraulic network

The hydraulic network is that nodal system in which the mass, momentum, and simplified energy equations are solved. A plenum is formed during discretisation of the length increment. Physically, a plenum can be a complex cavity with two or more links being connected to it. But it is assumed there that all changes inside the plenum occur simultaneously. Equation (5) is integrated over the boundary areas of the plenum:

$$\frac{\partial \rho}{\partial t} = - \frac{1}{V} \int_{(\text{Plenum})} dm \qquad (22)$$

Equation (9) is rewritten using equation (8) and (9) and writing $q_v = 0$ (adiabatic wall, no internal heat generation).

$$c_v \frac{\partial}{\partial t}(\rho T) = - \frac{c_p}{V} \int_{(\text{Plenum})} d(mT) \qquad (23)$$

The links are subdivided into nodes of uniform geometry where mixed mean values can easily be calculated. Now we can integrate the momentum equation along the link in which a temperature distribution is calculated by the other nodal system. By definition, the mass flow is uniform along the link. Taking all terms available we get:

$$\frac{\partial m}{\partial t} = \frac{-\int_{(\text{Link})} F dp + m^2 \int_{(\text{Link})} \frac{d(\rho F)}{(\rho F)^2} - g \int_{(\text{Link})} \rho F \sin\gamma \, dx - \int_{(\text{Link})} K_v F \, dx}{\int_{(\text{Link})} dx} \qquad (24)$$

By the procedures leading to the equations (21),(22),(23), (24) a number of simplifications was made. First, by separating the model into two different nodal system, shock waves cannot be calculated. The energy equation in the helium neglects mass inertia, dissipation, and compressibility. The latter effect is considered in the hydraulic network allowing to reproduce this effect by $\partial p/\partial t$ in the energy equation of helium. The main simplification of the hydraulic network is the reduction to a nodal system with the independent variables uniform inside these nodes.

4.3 The equations describing the energy release of the core

In that part of the structure material which is formed by fuel pellets, the term q_v in equation (18) is not zero. For the steady state at the design point many calculations have been performed /1/ to obtain the power distribution in the core and blanket. During transient calculations the power is supposed to change simultaneously at all points so that the point kinetics equations ensure a sufficient precision.

$$\frac{dv}{dt} = \frac{\rho_v - \beta}{l} v + \sum_{i=1}^{6} \lambda_i c_i \, , \qquad (25)$$

$$\frac{dc_i}{dt} = \frac{\beta_i}{l} v - \lambda_i c_i \, , \qquad (26)$$

Here, v is the number of neutrons, ρ_v the reactivity, β the effective part of delayed neutrons, β_i the effective part of the delayed neutrons in group i, l the effective life-time of the prompt neutrons, λ_i the decay constant, and c_i the concentration of the precursors of group i. The number of neutrons is proportional to the reactor power. Thus, we normalize with values of the design point having the index 0

$$\frac{dc_{io}}{dt} \equiv 0 \rightarrow c_{io} = \frac{\beta_i \, v_o}{\lambda_i \, l} \qquad (27)$$

After some manipulations we obtain

$$\frac{d}{dt} \left(\frac{v}{v_o} \right) = \frac{\rho_v - \beta}{l} \frac{v}{v_o} + \sum_{i=1}^{6} \frac{\beta_i}{l} \frac{c_i}{c_{io}} \qquad (28)$$

$$\frac{d}{dt} \left(\frac{c_i}{c_{io}} \right) = \lambda_i \frac{v}{v_o} - \lambda_i \frac{c_i}{c_{io}} \qquad (29)$$

The reactivity is calculated as a function of the effective multiplication factor k

$$\rho_v = \frac{k - 1}{k} \qquad (30)$$

The reactor core is subdivided into 6 volumes to calculate the Doppler feedback, four of which stand for the different zones of enrichment, one stands for the axial blanket and one for the radial blanket. Assuming a constant weighting factor W_i for those volumes, the feedback is calculated by the average pellet temperature T_i in that volume

$$\frac{1}{k_i} \frac{\partial k_i}{\partial T_i} = W_i \frac{K_{Di}}{T_i} \qquad (31)$$

and the total is found by the summation of all k_i. The axial expansion feedback is calculated by the average cladding temperature T_c of the whole core.

$$\frac{1}{k} \frac{\partial k}{\partial T_c} = K_A \qquad (32)$$

The radial expansion feedback is a function of the average inlet temperature T_1 into the core being that of the reactor inlet plenum

$$\frac{1}{k} \frac{\partial k}{\partial T_1} = K_R \qquad (33)$$

The actual average helium density variation in the core is compared to the density at the design point, ρ_o, to form the helium density feedback.

$$\frac{\partial k}{\partial \rho} = \frac{K_H}{\rho_o} \qquad (34)$$

Any form of control rod or shut-down rod reactivity can be inserted. A rectangular integration method is normally used with the same time step as that used in the calculation of

pellet temperatures, but the code allows to implement the main
AIREK subroutine /5/ with a higher order of integration method.
In case of reactor scram the shut-down heat is calculated
following the equations of /1/

$$\frac{N_{Core}}{N_{Core\ o}} = \left[\left(\left(\frac{N}{N_o}\right)_{28} + \left(\frac{N}{N_o}\right)_{38}\right)\frac{N_{Core\ Fission\ o}}{N_o} + \left(\frac{N}{N_o}\right)_{37}\frac{BR_{Core}}{BR_{total}}\right]\frac{N_o}{N_{Core\ o}}$$

(35)

$$\frac{N_{Blanket}}{N_{Blanket\ o}} = \left[\left(\left(\frac{N}{N_o}\right)_{28} + \left(\frac{N}{N_o}\right)_{38}\right)\frac{N_{Blanket\ Fission\ o}}{N_o} + \left(\frac{N}{N_o}\right)_{37}\right.$$

(36)

$$\left.\frac{BR_{Blanket}}{BR_{total}}\right]\frac{N_o}{N_{Blanket\ o}}$$

$\left(\frac{N}{N_o}\right)_{28}$ is the solution of equations (28) and (29).

The power due to the decay of breeding products of U_{239} and
Np_{239} is given in /1/

$$\left(\frac{N}{N_o}\right)_{37} = 0.0042\ e^{-4.9149\times10^{-4}t} + 0.0029\ e^{-3.4873\times10^{-6}t}$$

(37)

For the decay of the fission products, /6/ calculates

$$\left(\frac{N}{N_o}\right)_{38} = a_N\ t^{-b_N}$$

(38)

with the following list of constants:

t	a_N	b_N
< 10 sec	0.0603	0.0639
10 sec - 150 sec	0.0766	0.1807
> 150 sec	0.1301	0.2834

Fig.5 shows the variation of power generated with time after the scram by a -7$ insertion. It is obvious that the power reduced by the power of the design point is always higher for the blanket than for the core.

An additional feature of feedback calculation can be considered by calculating the reactivity effects of moving steel claddings. 141 different reactivity worths (fig.12) were calculated by the DIXI-code /7/ but the model of clad motion is still too coarse to yield realistic results of the reactivity feedback in case of a partial melt-down of the cladding material. In the example, a general tendency can be seen when using the reactivity worths of the DIXI-code.

4.4 The equations describing the helium circulator

The helium circulator has to be connected directly to an entrance and exit plenum. Tables containing steady-state values are used, correlating the normalized pressure difference and the normalized volume. Non-steady phenomena /8/ can be neglected because the volumes and heat capacities in the machine are small compared with adjacent loop components. The tables given by /9/ are used to interpolate the volume flow as a function of the speed of the shaft and the pressure difference between entrance and exit plena. For the energy balance of the shaft the energy required to run the circulator is also read from the tables. With respect to the stall limit the original tables show a stepwise change in volume flow down to zero. For the numerical solution in the nodal system of the hydraulic network this would impose severe restrictions on stability. Originally, a hysteris effect was calculated when the stall limit was exceeded and normal operation condition was reached again. This often leads to self-induced oscillations of the hydraulic network; this is too unrealistic because of lack of a multi-dimensional model with a high number of nodes.

Considering the stand-still of the circulator, it should be possible to calculate negative volume flows in case of malfunctioning of the non-return valve. In analogy to the calculation of the mass flow through a labyrinth packing /10/ the following correlation is used with the index 1 at the entrance, and the index 2 at the exit.

$$\frac{m}{F} = K \sqrt{\frac{\rho_1}{p_1} (p_1^2 - p_2^2)}$$
(39)

The constant K has to be selected such that a smooth transition to small numbers of revolutions is possible. By transformation of the original tables it is possible to calculate negative volume flows, even at any speed of the circulator, if the imposed pressure difference is high enough. The functions of negative volume flows at finite speed are similar to the function at zero speed. Fig.6 shows the pressure differences plotted versus the volume flow as it is usual for circulator diagrammes. In order to avoid normalized data, the normalizing reactor conditions at the entrance to the circulator are used, i.e. the inlet temperature is 546 K and the inlet pressure 115 bar. To adjust the resultant volume flow to the special needs of the loop, it can be multiplied by a constant, thus reaching the conditions of the design point. In the figure the outstanding curve representing the speed of 0 to 30 rpm leads to high negative volume flows for high pressure differences; for graphic representation it is reflected at the ordinate for the pressure difference values being greater than 10^{-2}. For the rest of the curves it should be noted that there is always a negative gradient and a smooth transition from one operation condition to the next. Therefore, points of the stall limit are not shown explicitly.

4.5 The equations describing the main steam turbine

The secondary loop is only simulated between the feed-water pumps and the main steam turbine. Thus, the inlet conditions of the steam turbine are the boundary conditions of the model. The speed of the turbine is constant as it is a function of the grid frequency. The simplified conelaw with index 1 for the entrance condition, index 2 for the exit condition, and index 0 for the design point can be written

$$\frac{\dot{V}_1}{\dot{V}_{10}} \sqrt{\frac{T_{10}}{T_1}} = \sqrt{\frac{1-(p_2/p_1)^2}{1-(p_{20}/p_{10})^2}} \tag{40}$$

For the design point $p_{20}/p_{10} \ll 1$, and for all conditions $p_2/p_1 \ll 1$ because otherwise the turbine would be by-passed. This leads to

$$\dot{V}_1 = \dot{V}_{10} \sqrt{\frac{T_1}{T_{10}}} \tag{41}$$

The mass flow $\dot{m}_1 = \dot{V}_1 \rho_1$ into the turbine is known by the mass balance in the steam generator so that the density ρ can be calculated by iteration, using the steam tables:

$$T_1 = T(\rho_1, h_1) \tag{42}$$

4.6 The equations describing the helium circulator turbine

The helium circulator turbine is directly connected to the helium circulator. The operation conditions are read from tables /9/ giving the normalized pressure difference and the normalized power as a function of the normalized speed and the normalized mass flow. The pressure difference for choked flow conditions is calculated and the mass flow is limited if those conditions are reached.

Fig.7 shows the power generated by the circulator turbine as a function of the mass flow. The normalizing factor is the inlet pressure enthalpy which has been held constant. The outlet pressure is neither changed.

4.7 The equations describing the pressure drops in helium

In equation (2) the force per volume K_v is introduced to allow for technical correlations of the forces acting on the adjacent walls. Those correlations are given for steady-state conditions. It has been investigated in /4/ how great the error would be, using a one-dimensional model under steady-state condition and rapidly changing Reynolds numbers in a turbulent flow. It is said that for a decelerated flow the transient friction factor is only slightly smaller than the steady-state friction factor. For the accelerated flow the friction factor can rise rapidly for a short period, but as the term of inertia is bigger than that of the friction at the wall, the error due to the steady-state friction factor calculation is reasonably small, although the transient value ($Re = 10^4$ to 10^5) is increased by 60% for a short period in comparison with the steady-state value. For the stepwise deceleration from $Re = 10^5$ to 10^4 the error is well below 5%.

The steady-state fluid flow in a horizontal tube of uniform cross-sectional area leads to a pressure drop correlated by

$$\frac{dp}{dx} = - K_v = \frac{\lambda}{d_h} \frac{\rho}{2} w \, | w |$$

(43)

With λ being the Weisbach friction factor and d_h the hydraulic diameter of the tube. The pressure drop at orifices and diverse blockades is

$$\frac{dp}{dx} = - K_v = \frac{\zeta}{dx} \frac{\rho}{2} w \, | w |$$

(44)

with ζ being the drag coefficient.

For those parts of the loops for which design parameters have not been fixed thoroughly or which are not important with respect to pressure drop, the standard correlations are used, i.e. for laminar flow (Re < 2300)

$$\lambda = 64/\text{Re} \tag{45}$$

and for turbulent flow (Re > 2300)

$$\lambda = 0.3164/\text{Re}^{0.25} \tag{46}$$

Empirical ζ-values are found by adjusting the steady-state conditions at the design point of the reactor loops.
For the smooth part of reactor core pins /11/ gives the laminar friction factor as a function of the pin diameter, the pitch of the hexagonal bundle, and the Reynolds number. The data given are approximated by the analytical function for laminar flow:

$$\lambda = \frac{88 + 70 \left(\frac{p_s}{d_s} - 1\right) - 45 \ \exp\left(-10.2 \left(\frac{p_s}{d_s} - 1\right)\right)}{4 \ \text{Re}} \tag{47}$$

In turbulent flow the correlation for the smooth part of the pin is given by /12/

$$\lambda = 4(1.036 + 0.054 \left(\frac{p_s}{d_s} - 1\right))(0.0014 + \frac{0.125}{\text{Re}^{0.32}})(1-\exp \left(\frac{1 - \frac{p_s}{d_s}}{0.0265}\right)) \tag{48}$$

For the smooth part of the pin the transition region between laminar and turbulent flow ($10^4 > \text{Re} > 10^3$) is simplified by assuming that the higher value of λ calculated in (47) or (48) is valid. Parts of the pins are roughened by transversal ribs for which /13/ gives the correlation

$$\sqrt{\frac{8}{\lambda}} = 2.5 \ \ln \left(\frac{1.05 \ p_s - d_s}{2 \ h_R}\right) + R(h^+) - \frac{3.75 + 1.31 \frac{p_s}{d_s}}{1 + 1.05 \frac{p_s}{d_s}} \tag{49}$$

Here the function $R(h^+)$ of the non-dimensional roughness height

$$h^+ = \frac{h_R m}{\eta\, F} \sqrt{\lambda/8} \qquad (50)$$

which is similar to the usual Reynolds number is introduced to take into account deviations of the conditions in the viscous sub-layer next to a rough surface from those next to a smooth surface.

For fully rough flow ($h^+ \geqslant 100$) the values of $R(h^+)$ are no longer a function of h^+. This asymptotic value can be calculated if the geometrical data of the roughness are known.

Although the evaluation of $R(h^+)$ as a function of the height, width, and pitch of roughness can be automated, it has been found neccessary to compare it with those of similar cases. For the present two-dimensional roughness (transversal ribs), having a height of $h_R = 0.1$ mm, a width of 0.1 mm, and a pitch of 0.7 mm, the equation reads

$$R(h^+) = R_c(h^+) = 5 \qquad (51)$$

For the transition region ($h^+ < 100$) a supplement to equation (51) is used to allow for the variation of $R(h^+)$ with h^+ (see /14/)

$$R(h^+) = R_c(h^+) - 0.33 + \frac{33}{h^+} \qquad (52)$$

The laminar condition is reached when $R(h^+)$ resulting from (52) is greater than the corresponding value resulting from

$$R(h^+) = 2.5 \ln h^+ + 5.5 \qquad (53)$$

At this interface the lowest value of (52) or (53) is used. As the fluid can also become stagnant and this would not be

matched by equation (53), the friction factor at smooth surfaces is taken from equation (47) for $h^+ < 10^{-5}$ because the roughness has no effect in laminar flow, which can be seen indirectly from equation (53), too.

4.8 The equations describing the heat transfer in helium

In analogy to the determination of K_v in equation (2) the heat transfer per volume in equation (3) is used to take into account the heat flux from the adjacent wall

$$q_v = \frac{\alpha \ (T_{Wall} - T)}{V} \cdot F_b \qquad (54)$$

using F_b for the wetted surface of the wall, α for the heat transfer coefficient, and T for the mixed mean temperature of the fluid. The Nusselt-number defined as

$$N_u = \frac{\alpha d_h}{k_w} \qquad (55)$$

is correlated for steady-state flow. /4/ gives survey of the errors using these correlations in a one-dimensional calculation for turbulent flow. In case of deceleration, the transient heat transfer coefficient is always very close to the steady-state coefficient. In an accelerated flow the heat transfer coefficient drops fast in the beginning but the time required to reach a new steady-state is very short in a helium cooled channel. The heat capacity of the fluid is small compared to that of the wall. Both effects result in the validity of a quasi-static energy equation although - for a stepwise change of the Reynolds number from 10^4 up to 10^5 - the heat transfer coefficient drops by about 40% over a short period.

The turbulent Nusselt number in the smooth part of a pin bundle is approximated by that for a turbulent flow (Re > 5000) of an equivalent annulus /15/

$$N_u = 0.018 \left(\frac{r_o}{r_1}\right)^{0.16} Re^{0.8} Pr^{0.4} \left(\frac{T_{wall}}{T_1}\right)^{-0.2} \left(1 + \frac{r_o}{r_1}\right)^{0.2} \qquad (56)$$

T_1 being the temperature at the core entrance and r_o/r_1 the ratio of the outer to inner radius of the annulus. The same correlation can be used for a normal tube outside the core by taking $r_o/r_1 = 1$, $T_{wall}/T_1 = 1$, $1 + \dfrac{r_o}{r_1} = 1$.

The Nusselt number for laminar flow (Re < 3000) in smooth bundles is given in /16/ by a graph which is correlated by the following function:

$$Nu = 7.2 + 8 \left(\frac{P_s}{d_s} - 1 \right) - 7.2 \exp \left(-8.5 \left(\frac{P_s}{d_s} - 1 \right) \right) \tag{57}$$

In the tubes outside the core the laminar Nusselt number is assumed to be 4.364. At the interface of the upper axial blanket and the core region the heat flux from the wall is increased rapidly. The velocity profile at that point has already been developed but a new temperature profile is formed leading to effects which the current one-dimensional quasi-static energy equation neglects. These errors are much higher for laminar flow because the fully developed profiles differ much more from a uniformly shaped profile than in a turbulent flow. In the thermal entry length the Nusselt number is higher and the value of equation (57) is multiplied by

$$\left(\frac{\left(\frac{r_o}{r_1} \right)}{0.00062} \right)^{-0.193 + \left(\frac{0.122}{x} \right)^{0.148}}$$

given in /17/ with $x = \dfrac{y}{d_h Re Pr}$, and y being the axial length starting at the beginning of the core region. In the transient flow between turbulent and laminar conditions the Nusselt number is correlated by

$$Nu = a \ Pr^{0.4} \left(\frac{T_{wall}}{T_1} \right)^{b} \left(\frac{r_o}{r_1} \right)^{c} \left(1 - \frac{r_o}{r_1} \right)^{b} \tag{58}$$

which is a variation of equation (56) with the values of a,b and c linearly interpolated between those for Re = 3000 and Re = 5000 given in the chart below.

	Re=3000	Re=5000
a	$Nu_{laminar}$	$0.023\ Re^{0.8}$
b	0	- 0.2
c	0	0.16

For the rough region of the core pin the turbulent Nusselt number is given in /14/ as a function of the parameters mentioned in the last chapter

$$\frac{Nu}{Re\ Pr} = \frac{\lambda/8}{1 + \sqrt{\lambda/8}(G(h^+) - R(h^+))} \qquad (59)$$

The function $G(h^+)$ of the normalized roughness height h^+ describes that part of the heat transfer phenomenon that takes place in the viscous sub-layer next to the wall with the artificial roughness. It is given by /14/

$$G(h^+) = (3.0 + 0.3\ (R(h^+) - 0.4\ \ln \frac{100}{f}))\ (h^+)^{(0.32-0.017(R(h^+)-0.4\ \ln \frac{100}{f}))} \qquad (60)$$

$$\cdot\ Pr^{0.44}\ \sqrt{\frac{T_{wall}}{T_{Bulk}}}\ \left(\frac{100}{f}\right)^{0.053}$$

with $f = (r_o - r_1)/h_R$ as a geometric factor of the equivalent annulus, r_o and r_1 being the outer and inner radiuses, respectively. To avoid iteration, the time-dependent variables of the last time step are used.

If the flow reaches laminar conditions, the Nusselt number of equation (59) is compared with that of equation (57) and the higher one is used.

In the transition region, h^+ might drop to values smaller
than 50, but $G(h^+)$ is calculated with the smallest h^+-value
to be 50, because $R(h^+)-0.4 \ln \frac{100}{f}$ is defined to be the
asymptotic value in fully rough flow of $R(h^+)_{01}$, which is
the value of $R(h^+)$ for $f = 100$.

4.9 The equations describing the heat transfer in the steam loops

In the energy equation of a steam node (see chapter 5.2),
ω_D is a function of the heat transfer coefficient, α, at the
peripheral wall. Water runs through the liquid, saturated
and superheated states during its stay in the secondary
loop. While α is a function of flow parameters like the
Reynolds number for the liquid and superheated states, it
is a function of the amount of heat exchanged at the wall
for the saturated state. For the latter phenomenon an
iteration produce will be necessary to calculate α.

The interfaces of these three states can change their positions
while transient problems are calculated. Several sophisticated
methods can be used and a definition of more than three kinds
of α-correlations is possible /18/. But here, the secondary
loop is of minor importance and, looking at the heat resistance
between water and helium, this is a strong function of the
heat transfer coefficient of the helium side while being a
weak function of that on the water side. Thus, the interfaces
of the three α-correlations are changing discontinuously in
such a way that they always coincide with node boundaries.
The interfaces are obtained by comparing the actual water
enthalpies with the two which delimit the saturated state
at the pressure prevailing. The α-correlations for the three
major states are /19/, /20/ and /19/:

$$\alpha_{water} = a\ Re^b\ Pr^c\ \frac{k_w}{d_h} \tag{61}$$

$$\alpha_{boiling} = d(eq)^f\ (gp)^h \tag{62}$$

$$\alpha_{steam} = x\ Re^y\ Pr^z\ \frac{k_w}{d_h} \tag{63}$$

with the following constants:

a	b	c	d	e	f	g	h	x	y	z
0.024	0.8	0.33	0.002163	859.85	0.72	0.0101972	0.24	0.024	0.786	0.45

and with k_w being the thermal conductivity, d_h the hydraulic diameter, and Pr the Prandtl number. Equation (62) is not homogenous with respect to the dimensions; the heat flux q must be given in kW/m^2, the pressure in kJ/m^3 and the heat transfer coefficient in $kW/(m^2K)$.

For water an additional heat flux due to sub-cooled boiling has increased considerably the accuracy of the results.

If the wall temperature is higher than the saturation temperature of the adjacent water, the heat flux due to convective heat transfer is augmented by a boiling term

$$q_{total} = \alpha_{water}\ (T_{Wall} - T_{H_2O}) + \alpha_{boiling}\ (T_{Wall} - T_{sat}) \tag{64}$$

T_{sat} being the saturation temperature of H_2O at the present pressure.

To accelerate convergence when calculating the boiling phase, the following procedure is coded. The energy balance between a steam and a wall node leads to the evalution of the heat flux.

$$q = \frac{T_{wall} - T_{H_2O}}{m + \dfrac{n}{\alpha_{boiling}}} \tag{65}$$

with m and n being geometrical constants.

The pressure stays constant during the iteration procedure so that

$$\alpha_{boiling} = d(eq)^f \ i \tag{66}$$

with $i = (gp)^h$. The combination of both equations results in

$$m\alpha_{boiling}^{\frac{1}{f}} + n\alpha_{boiling}^{\frac{1}{f}-1} = (di)^{\frac{1}{f}} \ e \ (T_{wall} - T_{H_2O}) \tag{67}$$

This equation can be solved by the approximation $\frac{1}{f} \approx 1.5$ and leads to the first guess in the iterative procedure for the evalution of $\alpha_{boiling}$.

4.10 The equations describing the energy balance of the turbo-machines

The mechanical power of the main steam turbine has no effect on the transient behaviour of the reactor loops. Thus, an energy balance must be calculated only for the shaft of the helium circulator-circulator turbine. The angular velocity ω of that shaft varies with the time

$$\theta \frac{d\omega}{dt} = M \tag{68}$$

θ being the mass moment of inertia, and M the sum of the momenta acting on the shaft. The data for the turbo-machines give the power as a function of the pressure difference and speed of the shaft; so M has to be evaluated by

$$M = \frac{N}{\omega} \tag{69}$$

with N being the sum of the turbo-machine powers.

The value of N is supplemented by that of the friction forces acting on the water - lubricated shaft. This is correlated by

$$N = N_o \omega^a \qquad (70)$$

with N_o and a being constant.

An explicit solution is used by taking the values of the right hand side of equation (68) as function of the last time step.

5. The solutions

5.1 The solution of the energy equation in a helium node

Equation (19) describes the variation of the helium temperature along the axis of a tube with constant mass flow. When discretising the coordinate along the axis, elements of the fluid and the adjacent wall are formed so that each wall element is adjacent to only one fluid element. This can be obtained by transformation of the coordinates as well.

Figure 8 shows such a node which is Δx long. The wall temperature is uniform over x and gives one boundary condition of the system. The initial condition is the temperature distribution in the fluid between the inlet temperature T_{EL} and the exit temperature T_{AL} of the last time step, where the index L shows that the time has been set $t=0$.

We now ask for the outlet temperature at $t = \Delta t$, if the wall temperature is changed stepwise at $t = 0$ and the fluid inlet temperature and the pressure are changed linear during Δt $(\dot{T}_E = dT_E/dt,\ \dot{p} = dp/dt)$. When defining a wall temperature combined with, $\dot{p}$, the pressure ramp, $T'_{Wall} = T_{Wall} + \dfrac{1}{\omega_R \rho c_p}\ \dot{p}$, and $\omega_R = \dfrac{1}{\rho F c_p R_w}$, equation (21) can be rewritten

$$\frac{\partial T}{\partial t} + w\,\frac{\partial T}{\partial x} = \omega_R\,(T'_{Wall} - T) \tag{71}$$

$$\text{with } T'_{Wall} = \begin{cases} T_{Wall\ o} & t \leq 0 \\ T_{Wall\ 1} + \dfrac{\dot{p}}{\omega_R \rho c_p} & t > 0 \end{cases} \quad \text{and } T(x=o) = \begin{cases} T_{EL} & t \leq 0 \\ T_{EL} + \dot{T} \times t & t > 0 \end{cases}$$

Solving equation (71), we separate into a steady-state part (index st) and a transient part (index tr):

$$T(t,x) = T_{st}(x) + T_{tr}(t,x) \tag{72}$$

By this we obtain an ordinary differential equation

$$w \frac{d\,T_{st}}{dx} = \omega_R \left(T'_{Wall} - T_{st} \right) \tag{73}$$

with
$$T_{st} = \begin{cases} T_{AL}, & x = \Delta x \\ T_{EL}, & x = 0 \end{cases}$$

and
$$T'_{Wall} = T_{Wall\ o}$$

and a partial differential equation

$$\frac{\partial T_{tr}}{\partial t} + w \frac{\partial T_{tr}}{\partial x} = \omega_R \left(T'_{Wall} - T_{tr} \right) \tag{74}$$

with
$$T_{tr}(x=0) = \dot{T}_E t \qquad t > 0$$

and
$$T'_{Wall} = \begin{cases} 0 & t \le 0 \\ T_{Wall\ 1} + \dfrac{\dot{p}}{\omega_R \rho c_p} - T_{Wall\ o} = T_{Wall\ tr} & t > 0 \end{cases}$$

The solution of equation (73) gives the temperature distribution which would be obtained for the steady state with uniform wall temperature.

$$T_{st}(x) = T_{Wall\ o} - \left(T_{Wall\ o} - T_{EL} \right) e^{-\frac{\omega_R}{w} x} \tag{75}$$

Equation (74) is transformed into the Laplace space with s being the independent variable and T_{tr}^{t} the Laplace transform of T_{tr}

$$s\,T_{tr}^{t} + w \frac{d}{dx} T_{tr}^{t} = \omega_R \left(\frac{T_{Wall\ tr}}{s} - T_{tr}^{t} \right) \tag{76}$$

with
$$T_{tr}^{t}(x=0) = \frac{1}{s^2} \dot{T}_E$$

Integration over the space leads to

$$T_{tr}^{t} = \frac{\omega_R}{s(s + \omega_R)} T_{\text{Wall tr}} + \left(\frac{\dot{T}_E}{s^2} - \frac{\omega_R}{s(s + \omega_R)} T_{\text{Wall tr}} \right) e^{-\frac{s + \omega_R}{w} x} \qquad (77)$$

When retransforming from the Laplace space, the influence of the finite transport time becomes visible. This transport time is a result of the convection velocity w of the fluid. For $t \leq \frac{x}{w}$ we find

$$T_{tr}(t,x) = (1 - e^{-\omega_R t}) T_{\text{Wall tr}} \qquad (78)$$

and for $t > \frac{x}{w}$ we find

$$T_{tr}(t,x) = (1 - e^{-\omega_R t}) T_{\text{Wall tr}} + \dot{T}_E (t - \frac{x}{w}) e^{-\frac{\omega_R}{w} x} - (1 - e^{-\omega_R (t - \frac{x}{w})}) e^{-\frac{\omega_R}{w} x} T_{\text{Wall tr}} \qquad (79)$$

Calculating the energy exchange with the adjacent wall we have to discretise the time, which leads to the time step Δt. We now want to know the exit temperature T_A of a node after such a time step. Using equation (72), we obtain for $\Delta t \leq \frac{\Delta x}{w}$

$$T_A = T(t=\Delta t, x=\Delta x) = T_{\text{Wall 1}} - (T_{\text{Wall 1}} - T^*) e^{-\omega_R \Delta t} + \frac{\dot{p}}{\omega_R \rho c_p} (1 - e^{-\omega_R \Delta t}) \qquad (80)$$

with $T^* = (T_{AL} - T_{EL} e^{-\frac{\omega_R}{w} \Delta x}) \dfrac{1 - e^{-\frac{\omega_R}{w} (\Delta x - w\Delta t)}}{1 - e^{-\frac{\omega_R}{w} \Delta x}} + T_{EL} e^{-\frac{\omega_R}{w} (\Delta x - w\Delta t)}$

and for $\Delta t > \frac{\Delta x}{w}$

$$T_A = T_{\text{Wall 1}} - (T_{\text{Wall 1}} - T^*) e^{-\omega_R \frac{\Delta x}{w}} + \frac{\dot{p}}{\omega_R \rho c_p} (1 - e^{-\omega_R \frac{\Delta x}{w}}) \qquad (81)$$

with $T^* = T_{EL} + \dot{T}_E (\Delta t - \frac{\Delta x}{w})$

The space and time discretised system is linked in space by the entrance temperature T_{EL} being equal to the exit temperature T_A of the neighbour node at the last time step. The neighbouring element, which lies always downstream, is chosen by looking

whether the mass flow is negative or positive.

Equations (80) and (81) are solutions for the exit temperature, which do not use extrapolation methods with minor stability when the convection velocity reaches zero. The first lines of (80) and (81) have the same form as equation (75). They show an exponential change of temperature with x allowing for a pressure ramp which is given as a boundary condition. The time increment responsible for the temperature variation is either Δt (equation (80)) or $\frac{\Delta x}{w}$ (equation (81)). The start-up condition is expressed by the temperature T^*.

Figure (8) shows T^* for both cases. Regarding the figure for $w\Delta t \leq \Delta x$, T^* is the temperature of that fluid particle that was at the place $x = \Delta x - w\Delta t$ for $t = 0$, when the temperature distribution was characterized by $T_{EL} - T_{AL}$. For $w\Delta t > \Delta x$, this fluid particle was outside the node considered. In analogy to equation (80) T_{EL} would be obtained by extrapolation over the boundaries of the node. Instead of this instable procedure equation (81) shows how T^* is formed by the boundary condition that T_E varies linear during Δt. A fluid particle starting at the point of T_E needs only $\Delta t = \frac{\Delta x}{w}$ to reach the position of the exit temperature T_A. The fluid particle is only traced while being inside the node.

5.2 The solution of the energy equation in a steam node

Neglecting the pressure variation with time and allowing for incompressibility and constant mass flow, equation (15) is reduced to

$$\frac{\partial i}{\partial t} + w \frac{\partial i}{\partial x} = \omega_D (T_{Wall} - T) \tag{82}$$

with $\frac{1}{\omega_D} = \rho F R_w$ see chapter 4.9. The enthalpy i and the temperature T are linked by steam tables. Separating into a steady state part (index st) and a transient part (index tr), we obtain

$$i(t,x) = i_{st}(x) + i_{tr}(t,x)$$

$$T(t,x) = T_{st}(x) + T_{tr}(t,x)$$

$$(83)$$

and

$$w \frac{di_{st}}{dx} = \omega_D(T_{Wall\ st} - T_{st})$$

$$(84)$$

with

$$i_{st}(x=\Delta x) = i_{AL}, \quad i_{st}(x=0) = i_{EL}, \quad T_{Wall\ st} = T_{wo}$$

and

$$\frac{\partial i_{tr}}{\partial t} + w \frac{\partial i_{tr}}{\partial x} = \omega_D (T_{Wall\ tr} - T_{tr})$$

$$(85)$$

with

$$i_{tr}(x=0) = i_E'\ t\ , \quad t > 0, \quad T_{Wall\ tr} = \begin{cases} 0, & t \leq 0 \\ T_{w1} - T_{wo}, & t > 0 \end{cases}$$

The entrance enthalpy varies linear with time because $i_E' = \frac{\partial i_E}{\partial t}$ = constant, and the wall temperature varies stepwise from T_{wo} to T_{w1}. It is necessary to state that one cannot avoid iteration because temperatures and enthalpies are linked by steam tables.

So, in the first step, the right-hand sides of equations (84) and (85) are kept constant. Convergence has to be obtained for the temperature calculated by the steam tables and that standing on the right-hand side of the equations.

The solution of equation (84) gives a linear variation of the enthalpy

$$i_{st}(x) = i_{EL} + \frac{\omega_D}{w} (T_{wo} - T_{st})\ x$$

$$(86)$$

Equation (85) is solved by the Laplace transformation in analogy to equation (76). Again the convection velocity is a major parameter. The energy equation is solved always inside the node considered. We obtain the transient part of the enthalpy:

$$i_{tr}(x,t) = \omega_D(T_{w1} - T_{wo} - T_{tr})\ t \qquad \text{for}\ 0 < t < \frac{x}{w}$$

$$i_{tr}(x,t) = \omega_D(T_{w1} - T_{wo} - T_{tr})\ t + (i_e' - \omega_D(T_{w1} - T_{wo} - T_{tr}))\ (t - \frac{x}{w})\ \text{for}\ t > \frac{x}{w}$$

$$(87)$$

The exit enthalpy $(x = \Delta x)$ for $t = \Delta t$ is a result of the combination of equations (86) and (87), using $i'_E = \dfrac{i_E - i_{EL}}{\Delta t}$

$$i_A = i_{EL} + \omega_D \Delta t \, (T_{w1} - T) + (i_{AL} - i_{EL})\left(1 - \frac{w\Delta t}{\Delta x}\right) \qquad \text{for} \quad w\Delta t \leq \Delta x$$

$$i_A = i_E + \omega_D \frac{\Delta x}{w}(T_{w1} - T) + (i_{EL} - i_E)\frac{\Delta x}{w\Delta t} \qquad \text{for} \quad w\Delta t > \Delta x$$

$$(88)$$

Because equation (86) gives a variation of the enthalpy linear with space, a mixed enthalpy i at $t = \Delta t$ can be defined by the arithmetic average of inlet and outlet enthalpies. In the evaluation of the mixed mean enthalpy as an average value between two time steps, a linear interpolation is used, too. The time and space averaged temperature is read from the steam tables using this enthalpy. This temperature is used to calculate the heat transfer from the wall which ends one iteration step.

5.3 Mixed medium temperatures in a helium node

To solve the equation for the heat flux from the wall a mixed medium temperature $\overline{T}$ is used. In the energy equation the parameters ω_R, ρ, c_p are found to be functions of that temperature. Evaluating the terms on the right-hand side of the momentum equation (24), the mixed medium temperature must be known, too. Equation (75) gives the steady state axial variation of the helium temperature in the node. Integration leads to

$$\overline{T} = T_{wall} - (T_{wall} - T_E)\frac{1 - e^{-\omega_R \frac{\Delta x}{w}}}{\omega_R \frac{\Delta x}{w}} \qquad (89)$$

Replacing T_w by means of equation (75) results in

$$\overline{T} = \frac{T_A - T_E \, e^{-\omega_R \frac{\Delta x}{w}}}{1 - e^{-\omega_R \frac{\Delta x}{w}}} - \frac{T_A - T_E}{\omega_R \frac{\Delta x}{w}} \qquad (90)$$

if $\omega_R \frac{\Delta x}{w}$ is less than 0.01, a linear interpolation can be used since T_A has nearly the same value as T_E:

$$\bar{T} = \frac{T_E + T_A}{2} \tag{91}$$

In the energy equation, the wall temperature is set constant during the time step. After having found a solution for the helium temperatures, the energy balance is performed inside the structure material. Using a simple explicit integration method with respect to time, an average temperature is found by linear interpolation between T of the last and the present time steps. The interpolated value is a boundary condition of the energy equations in the structure material.

If the helium node is bounded by walls of different temperatures, two parameters in the preceding chapter have to be evaluated differently:

$$\omega_R = \sum_i \frac{1}{\rho F c_p R_{wi}} = \sum_i \omega_{Ri} \tag{92}$$

$$T_{Wall} = \sum_i \frac{\omega_{Ri}}{\omega_R} T_{Wall\ i} \tag{93}$$

By this, the right-hand side of equation (71) is extended allowing more than one wall adjacent to the helium.

5.4 The wall to wall heat transfer

A gap exists between the fuel pellet and the steel cladding the size of which varies with space and time. Because analytical functions are not available, the value is considered to be constant. It must be uniform in each link and the equivalent heat transfer coefficient in the equation

$$q = \alpha \ (T_{pellet} - T_{clad}) \tag{94}$$

is supposed to be 10 kW/(m^{2}K) for all core links. This has to be connected to the system of equation (18).

A mixed mean temperature in the subassembly wall is calculated

allowing heat exchange by radiation between the cladding and the subassembly wall. To avoid a new procedure of solving the energy equation in the helium node, only the heat flux entering the subassembly wall is calculated. The heat flux to or from the pin's cladding is not changed; this procedure is on the safe side.

It can be expected that the error is small because radiation plays a minor role in the energy balance. The ratio of radiation surfaces is assumed to be 1, the black body constant is C, the emissivity is ϵ, the surface area is A, and the heat flux

$$q = \frac{C}{\frac{2}{\epsilon} - 1} A\left(\left(\frac{T_{clad}}{100}\right)^4 - \left(\frac{T_{subass}}{100}\right)^4\right)$$ (95)

5.5 The solution of the energy equation in the wall

It has been said in chapter 4.1 that the energy equation in the wall or in the pin with the adjacent pellet is solved in a one-dimensional form mainly because axial heat conduction is neglected.

Writing equation (18) in the form of finite differences (i-th node), and taking the backward difference scheme for the derivation of time (T_{iL} = temperature of the last time step), the heat conduction equation becomes

$$\frac{T_i - T_{iL}}{\Delta t} = \frac{a}{(\Delta r)^2} (T_{i+1} + T_{i-1} - 2T_i) + \frac{a}{2r_i \Delta r} (T_{i+1} - T_{i-1}) + \frac{q_v}{\rho c}$$ (96)

Solving it for a limited number of nodes leads to a system of linear equations with a tridiagonal matrix which can easily be inverted. If the time steps of this integration are different from that of the energy equation of the helium node, both results must be transformed in order to establish adequate boundary values for the complementary equations.

5.6 The solution of the equations governing the hydraulic network

The solution of the equations of chapter 4.2 is performed by an implicit method.

The right-hand sides of equations (22) and (23) show only the mass flow m as an independent variable. The temperature T is a parameter solved in the energy equation of a link. By substitution we can now reduce the system of equations (22), (23), (24) to only (24). The solution of (24) can simply be used to calculate (22) and (23) /21/.

The procedure of the implicit method can be reduced to the following lines while looking at a system of ordinary differential equations after discretisation of the space-coordinates

$$\frac{d}{dt} \vec{y} = \vec{f}_a (\vec{y}) \tag{97}$$

$\vec{y}$ is the vector of state and $\vec{f}_a$ the vector function. The vector function $\vec{f}_a$ will now be taken at the time t + dt where the vector has reached $\vec{y} + d\vec{y}$, transforming it into $\vec{f}_b$

$$\frac{d}{dt} \vec{y} = \vec{f}_b (\vec{y} + d\vec{y}) \tag{98}$$

Writing the right-hand side in terms of the original vector function

$$\vec{f}_b (\vec{y} + d\vec{y}) = \vec{f}_a + d \vec{f}_a \tag{99}$$

we get

$$\vec{f}_a dt = d\vec{y} - d \vec{f}_a dt \tag{100}$$

As $d\vec{f}_a$ is a function of the vector of state we can write

$$\vec{f}_a dt = B \, d\vec{y} \tag{101}$$

By inverting the matrix B with the elements $b_{ik} = - \dfrac{(\partial f_a)_i}{\partial y_K} dt$ and $b_{ii} = 1 - \dfrac{(\partial f_a)_i}{\partial y_i} dt$, we can find a solution for $\vec{y}$.

Equation (22) is now used to calculate the function of the density with m_n being a mass flow of one link ending in the plenum considered

$$f_{ai}(\rho_i) \equiv \frac{d\rho_i}{dt} = \frac{1}{V_i} \sum_{n=1}^{k} m_n \tag{102}$$

Using the procedure that leads from equation (97) to (100) and discretising the time we find

$$f_{ai}(\rho_i) \, \Delta t = \Delta \rho_i - \frac{\Delta t}{V_i} \sum_{n=1}^{k} \Delta m_n \tag{103}$$

In a similar manner, equation (23) is used with the help of (102)

$$f_{ai}(T_i) \equiv \frac{dT_i}{dt} = \frac{1}{\rho_i V_i} \sum_{n=1}^{k} (\kappa \, T_n - T_i) \, m_n \tag{104}$$

After some manipulations using (103) we obtain

$$f_{ai}(T_i) \left(1 - \frac{f_{ai}(\rho_i)}{\rho_i} \Delta t\right) \frac{\Delta t}{A_i} = \Delta T_i - \Delta t \sum_{n=1}^{k} \frac{B_n}{A_i} \Delta m_n \tag{105}$$

with $A_i = 1 + \dfrac{\Delta t}{\rho_i V_i} \sum_{n=1}^{k} m_n$ and $B_n = \dfrac{1}{\rho_i V_i} (\kappa \, T_n - T_i - f_{ai}(T_i)\Delta t)$

By equations (103) and (105) we have found correlations for $\Delta \rho_i$ and ΔT_i of the plenum considered. Using the ideal gas law we write

$$\Delta p_i = R \, T_i \, \Delta \rho_i + R \, \rho_i \, \Delta T_i \tag{106}$$

When writing the momentum equation for a link the pressure p_i and p_j of the adjacent plena are major parameters.

The finite increment of the mass flow function is now

$$\Delta f_{ak}(m_k) = \frac{\partial}{\partial p_i} (f_{ak}(m_k)) \Delta p_i + \frac{\partial}{\partial p_j} (f_{ak}(m_k)) \Delta p_j + \frac{\partial}{\partial m_k} (f_{ak}(m_k)) \Delta m_k \quad (107)$$

$f_{aK}(m_K)$ is defined in the well-known manner with the help of equation (24). Here, $\int F dp$ is a function of p_i and p_j; p^* is a pressure normalized with the value of $(p_i - p_j)$, L_x is the total length of the link, K_v is calculated by using (43) and (64):

$$f_{ak}(m_k) \equiv \frac{dm_k}{dt} = \frac{1}{L_x} \left(-(p_i - p_j) \sum_{(LINK)} F \Delta p^* - m_k |m_k| \sum_{(LINK)} \frac{\Delta(\rho F)}{\rho^2 F^2} \right.$$

$$\left. \tag{108}$$

$$- g \sum_{(LINK)} \rho F \sin\gamma \, \Delta x + m_k |m_k| \sum_{(LINK)} (\lambda \frac{\Delta x}{d_h} + \zeta) \frac{1}{2\rho F} \right)$$

If the link is formed by a helium circulator, the mass flow is a function of the pressures p_i and p_j, of the inlet temperature T_i and of the speed of the shaft Z_n. Friction losses in the tube leading to or from the circulators are neglected. Thus, in equation (107) the term with Δm_K has to be replaced by one with ΔT_i and a new one has to be added with ΔZ_n.

In analogy to the steps from (97) to (101) we find a system of equations using the substitution of (106) by (107)

$$\vec{f}_a(\vec{m}) \Delta t = B \, \Delta\vec{m} \quad (109)$$

The elements of $\vec{f}_a$ are different for a link with or without circulator.

The matrix B has n^2 elements for a model with n links. Figure 9 shows a matrix scheme for the reactor presently being simulated. The elements of the main diagonal describe the influence of the present link on itself; the rest of the non-zero elements of one row (or column) describe the influence of those links which are connected to the same plena as the link considered in the present row (or column).

In figure 9 the matrix has $n^2 = 400$ elements. Without the reduction procedure a number of 15 plena would have to be added and the matrix would have 2500 elements. Considering that an inversion of the matrix would need about n^3 operations, we find that by the present reduction over 90% of expenditure in terms of calculation has been avoided.

5.7 The determination of the steam mass flow

The space-dependent change of the mass flow in the secondary loop has only little effect on the conditions prevailing in the primary loop. The present calculation only allows for compressibility in the steam generator so that all mass flows adjacent to it are uniform. Large time-dependent changes are thus only results of changes in the boundary conditions, such as the feed water mass flow and conditions in the throttle valves. Although the steam-water velocity may change rapidly with time and space, the effect on the energy balance between the primary and secondary loops is small because the heat transfer coefficient on the H_2O-side is always considerably greater than that on the helium side, as mentioned before. Once the mass flows into and from the steam generator are calculated as functions of the pressure drops and feed water mass flows, an iteration is made over the mass inventory of the steam generator. Since the mass flow and pressure are known, the energy equation can be solved giving the boundary conditions for the next sets of mass flow calculations.

6.   The code

6.1   The PHAETON2 computer code

The code is written in FORTRAN IV and is run on an IBM/370-168. It is a stand-alone version which normally needs about 340 K storage in the go-step. Integration routines have not been optimized as many rectangular routines are used. Thus, CPU-times are rather long. Evidently, they depend considerably on the number of nodes which are specified by the model. Fig.10 shows a simplified flow chart of the main programme of the code. The code scheme is shown in fig.11. The subroutines of this scheme are described below.

1. AUS

Calculates the helium mass inventory and establishes a total energy balance for the core, the blower, and the heat exchangers. Saves the values of the last time step.
Calculates the hot-spot temperatures with constant hot-spot factors.
Calculates the maxima of the hot spot and nominal temperatures and saves the values for the variables to be plotted on an external plotter.
Saves the values for the variables to be plotted by BILDPL.
Prints out variables at a specified time.

2. BILDPL

Plots variables as functions of time using the printing unit. Up to 20 independent variables can be plotted in up to 20 charts allowing an arbitary number of variables in one chart.

3. CAUS

Prints out temperatures in the core and tells which cladding nodes have been molten.

4. CLPROP

Calculates the properties of the cladding material, such as density, specific heat capacity, thermal conductivity and thermal diffusivity.

5. COND

Solves the heat conduction equation in the core pins. If the clad is molten, it takes the surface temperature of the pellets adjacent to the helium flow. Calculates all temperatures in the pellet and clad.

6. DAMPF

Solves the energy equation in the secondary loops. Calculates in the order indicated the heat transfer coefficient H_2O-wall, the heat resistance between the nodes of the wall and fluid, the wall temperatures, the fluid enthalpies, and the fluid temperatures.

7. DWERT

Calls the PROPA subroutine and transfers variables into PHAETON2 dimensions. Calculates the density as a function of the specific volume of steam.

8. EIN

Reads and writes the input data, which are subdivided into constants and intial conditions. The constants define the reactor model and the geometrical configuration. They do not vary once a reactor model has been set up. The initial conditions define the vectors of data, the properties, and related variables needed to start up a run. They are given for all variables that are calculated directly by the transient phase of the code.

9. FDPD

Calculates the pressure drop in the secondary loops. Defines a mixed medium pressure in a H_2O node since the inlet pressure is known and the outlet pressure can be calculated.

10. FDWP

Solves the mass and momentum equations in the secondary loops.
Takes the mass flow to the main turbine of the last time step
as a first guess and calculates the pressure and densities
according to the guessed mass flow distribution with the
help of the subroutines FDPD, VENT2, PTUR and HTUR.
Calculates a new mass flow distribution by a mass balance in
the steam generator by knowing the new density distribution
by the subroutine FRD1, and the feed-water mass flow into the
steam generator which is a given boundary condition. Iterates
this procedure up to convergence of the mass flow distribution.

11. FKEFF

Calculates the rate of reactivity which is inserted by shut-down
rods. Knowing the reactivity feed-back by the FZKF subroutine,
it solves the point kinetics equations with six groups of
delayed neutrons. Calculates the shut-down heat distribution
in case of a scram and evaluates the relative power of the
reactor by taking into account all parts mentioned above.

12. FPRPL

Interpolates the helium node pressure linearly between the
values of the adjacent plena. Calculates the helium densities
as a function of these pressures and the temperatures. Provides
information about boundary conditions which are defined by the
user.

13. FPUMP

Calculates the enthalpy difference, the mass flow, and the
power of the helium circulator as functions of the adjacent
pressures and the inlet temperature. The subroutine with
tables included is given by General Atomic San Diego.

14. FRD1

Calculates the H_2O-densities as functions of the enthalpies
and pressures using DWERT subroutine. Defines the boundaries
of the wet steam phase by comparing the actual enthalpies to
those of the boundaries at the present pressure. Sets these

boundaries to be congruent with that of the nodal system.

15. FRIC

Calculates the Fanning friction factor of the helium flow for
the loops and for the core.

16. FWS1

Calculates the feed-water mass flow which is a boundary condition
defined by the user.

17. FWW

Calculates the integrals in the momentum equation of the helium
flow.

18. FZKF

Calculates the amount of reactivity due to Doppler, void, axial
expansion, and radial expansion feedbacks.
Takes into account the reactivity change if the steel cladding
is moved in case of partial melt-down.
Defines the medium temperatures and densities in the core which
must be known to calculate the reactivity feedbacks above.

19. GAUSS

Solves a set of linear equations by Gaussian elimination.

20. HEPROP

Calculates the properties of helium, such as the density, the
specific heat capacity, the thermal conductivity, the thermal
diffusivity, the dynamic viscosity, the Prandtl number and
the ratio of specific heats.

21. HTCOEF

Calculates the heat transfer coefficient of helium to wall for
the loops and for the core.

22. HTEMP

Solves the energy equation inside a helium node. Calculates the helium outlet temperature and the mixed medium temperature of a helium node. Evaluates the heat flux from helium to the adjacent wall. If only a wall with adiabatic external surface is given, the code calculates the temperature of this wall including the temperature of the subassembly wall in the core. If the wall faces the steam loops, the wall temperature calculation is performed by DAMPF.

23. HTUR

Calculates the inlet pressure of the main steam turbine as a function of the inlet enthalpy and the mass flow. This subroutine can be by-passed and the inlet pressure can be given by a function defined by the user.

24. IMPL

Solves the equations governing the hydraulic network of the helium loops. First calculates the mass flow through a given leakage in the PCRV and then establishes the characteristic matrix of the hydraulic network with the help of FWW and FPUMP. Calculates the mass flow variation in each link by inverting the matrix and then evaluates the densities and temperatures in the plena. Recalculates the mass flow through the circulators using directly the circulator tables. Evaluates average values with respect to time of the vectors of state in the plena for the energy balance in the links, which is done in the HTEMP subroutine.

25. KON

Reads in constants of the core subassemblies and calculates constants that must be known during transient calculations of the core and the primary and secondary loops. Prints out the main constants.

26. NETWORK

Examines the model that has been specified by the parameters
read in EIN and KON and prints out the errors if the model is
not consistent with the needs of the PHAETON2 code. Prints
out a graph showing the hydraulic network.

27. PAUS

Prints the values of a given vector.

28. POWER

Calculates the power per volume generated in the pellets.
A space-dependent distribution of the linear power in the
core is given which is multiplied by the relative power
calculated by FKEFF.

29. PRERR

Announces an error if the variable to be checked reaches
boundary values.

30. PROPA

Calculates the temperature, both limiting enthalpies of the
wet steam phase, the specific volume, and the specific heat
capacity of H_2O as a function of the enthalpy and the pressure
by interpolating the values in steam tables given by the
General Atomic Company San Diego. The limiting values for the
input data are:

$$207 \text{ kJ/m}^3 < \text{pressure} < 22700 \text{ kJ/m}^3$$
$$23.2 \text{ kJ/kg} < \text{enthalpy} < 15700 \text{ kJ/kg}$$

31. PLPROP

Calculates the properties of the core pellets, such as the
density, the specific heat capacity, the thermal conductivity,
and the thermal diffusivity.

32. PTUR

Calculates the outlet enthalpy, the inlet pressure, and the energy consumed by the helium circulator as functions of the inlet enthalpy, the outlet pressure, the mass flow, and the speed of the shaft. Interpolates the values in tables given by the General Atomic Company, San Diego. Takes into account choked flow and a parabolic characteristic of the circulator at stand-still. Thus extrapolates the tables down to negative flows.

33. RESERV

Punches and prints out values needed for initial conditions for any run to follow the present one.

34. TERP

Does Lagrangian interpolation of a dependent variable as a function of an independent variable, both given in the form of tables.

35. TRANS1

Transforms the values of the temperature gradients calculated in the nodal system of helium into the nodal system of the steam loops.

36. TRANS2

Transforms the values of the temperature gradients and the temperatures calculated in the nodal system of the steam loops into the nodal system of the helium loops.

37. TRIDIA

Solves a set of linear equations with a tridiagonal matrix.

38. VALUE

Does the Lagrangian interpolation of a dependent variable as a function of two independent variables by use of TERP.

39. VENT2

Calculates the inlet pressure of a control valve in the steam
loops as a function of the outlet pressure, the mass flow, and
the inlet enthalpy. The characteristic cross-sectional area
and the drag coefficient of the value must be known, too.

6.2 The model with four links in the core

Two models have been established to calculate the 1000 MWe
reactor of KWU. The first is characterized by four links
to analyse an average cooling channel around an average pin
in four different core positions. Fig.2 shows the model of
all coolant loops being calculated by the corresponding
version of the code. The four core links represent one channel
in the centre of the core allowing hot-spot calculations with
constant hot-spot factors, one average channel for both central
enrichment zones, one average channel for both peripheral
enrichment zones, and one average channel of the radial blanket.
Two loops are modelled, one representing 7 undamaged helium
loops and the other a damaged helium loop with adjacent steam
loops. Thus, a total of 157 helium nodes must be calculated.
Having 16 links, numbers 13 to 16 for the core, the hydraulic
network is calculated using the matrix of fig.9. The position
of the links outside the core is defined by the chart below.

Link - No.	connects	plenum No.	to	plenum No.
1		2		3
2		3		4
3		4		5
4		5		6
5		6		7
6		7		1
7		2		8
8		8		9
9		9		10
10		10		11
11		11		12
12		12		1

Each of the secondary loops has 44 nodes. There is always an adjacent wall to the nodes with a uniform temperature inside the wall, except for the core where a pin is subdivided into 13 radial segments two of which are modelling the steel cladding. Together with one segment of the subassembly wall 672 temperatures are calculated in the structure material of the core. The main features of the core can be looked up in fig.13.

6.3 The model with thirteen links in the core

The second model, of the 1000 MWe reactor of KWU has been built to concentrate the attention on a better core calculation. If one defines concentric rings of subassemblies, the total core and blanket is formed by 13 such rings, the innermost being the central subassembly of the core only. Each ring is now represented by a link which solves the equations for an average pin. The 8 loops outside the core cavity are represented by one loop allowing only simultaneous changes in all primary and secondary loops. In fig.3 the model is drawn in the same way as in fig.2. The pin radial nodes are reduced to 6 while the number of nodes in the cladding remains 2.

Since the 3 links of the radial blanket are not as important for calculation as that of the core region, they are subdivied into 7 axial segments only. With one node in the subassembly wall for each axial segment, 1128 temperatures are calculated in the structure material of the core. Core segmentation can be seen from fig.12 where one reactivity value is listed for each axial segment.

The model consists of 19 links, 13 of which have been already described. Links 1 to 6 are copied directly from the first model of fig.2. A total of 187 helium nodes are established.

6.4 Start-up conditions at the design point

The conservation equations in PHAETON2 are always time dependent. The initial conditions must be known before a dynamic run. When modelling a new reactor, the steady-state condition at the design point should be known, too. Otherwise, they have to be calculated before entering PHAETON2. Then, dynamic test runs begin to adjust parameters of the model in such a way that a steady-state is calculated and the values of the variables converge towards the design values. Simplifications of the model are preferably performed at those points which are of minor importance for the dynamic results. For example, the present versions neglect the influence of the temperature on the heat conductivity of the UO_2 pellet. Allowing for rising heat conductivities with rising temperatures, when passing beyond the values of 1900 K, the temperatures in the centre of the pellet come out lower than that of the PHAETON2 model. But the attention is mainly paid to the calculations of the cladding temperatures. The uncertaintes in obtaining a realistic value for the cladding-pellet gap resistance (the equivalent heat transfer coefficient is supposed to be 10 kW/m^2 grd) tend towards the same direction: temperatures in the pellet are overestimated, temperatures in the cladding are realistic. Fig.14 shows the temperatures of a pin in the centre of the core as a function of its axial position. Axial blanket values habe been ommitted.. In the first three nodes the temperature difference of helium to wall is higher than for the rest of the nodes because of the lack of a roughened cladding surface. Fig.15 shows the conditions in the heat exchangers of one of eight loops at the design point. The wall temperatures which have been ommitted are very close to the water temperatures except for the regions of superheated steam, especially in the resuperheater.

7. The accidents

7.1 The depressurization accident

One depressurization accident is discussed here, the description
of other accidents has been published already /1/, /2/, /3/.
The accident in question occurs when a leakage is assumed
that connects plenum number 11 (see fig.3) to the cavity of the
secondary containment, starting with time = 1 sec. This
containment is built around the PCRV and withstands an internal
pressure of about 3 bar. The failure of one of many small
penetrations through the PCRV results in a certain free area
the helium can pass through. Assuming no friction in this
passage an idealized hole is considered with a cross-sectional
area of 0.016 m^2. For the beginning of an accident the isotropic
flow will be choked so that the pressure within the secondary
containment in the boundaries of 1 bar to 3 bar has no influence
on the flow rate through the hole. When the critical pressure
ratio of helium (=2.05) occurs the pressure in the secondary
containment has already built up considerably. This is a function
of the volume available. To simplify the calculations the
pressure is supposed to remain constant at the maximum backup
pressure which is an important parameter. Its value is put
2.4 bar which is 2% of the helium pressure in the loop at the
design point. The critical pressure ratio is reached at
time = 67 sec when the total mass inventory of the primary loop
is still 4.8%. Thus, 9700 kg have been released into the secondary
containment. Assuming a mean temperature of 500 K, the volume of
the secondary containment must be 72000 m^3 to reach in time
2.4 bar of backup pressure. The PCRV has a total volume of
26000 m^3 so that 72000 m^3 are restrictive on the design
of the secondary containment. The leakage is opened at
time = 1 sec. Due to the leakage a maximum of 120 kg/sec helium
flows through the hole, which is 6.3% of the nominal mass flow
through the core. Fig.16 shows the output data for the
depressurization accident as function of time. Looking at the
pressures in the primary loops which differ very little with
space (the maximum total pressure drop is 6 bar) we see that
they are represented by only one line. They fall nearly

exponential with time. Thus, it has been useful to introduce
a time constant for depressurization, which is defined here
by that time interval during which the pressure drops to 37%.
The present time constant is consequently evaluated to be
20 sec. Pressure compensation at the leakage point is reached
at about time = 80 sec. During the whole accident, the mass
flow rate through the leakage is so small that the mass flows
in the damaged loop do not differ much with respect to their
position. The leakage mass flow is branched off just in front
of the helium circulator so that the machine has to work
against a higher pressure difference. This reduces the helium
output of plenum number 11 and thus leads to a reduction of
the pressure difference across the circulator until stabilization
occurs of the transient effects in the damaged loop. But for the
main energy balance in the core the variation of the total mass
flow of all loops as a function of control activities is more
important. The reactor is scrammed, the signal being delayed
by 1 second. Shut-down rods fall by gravity but here a linear
variation of reactivity with time is assumed. So a time lag of
0.15 seconds is introduced to cope with acceleration effects,
the results being a linear insertion of -10.8 $/sec between
time = 2.15 sec and time = 2.80 sec, which leads to a total
reactivity of -7 $. Fig.16 shows the normalized power of the
core and the blanket as a result of this shut-down. In the
secondary loops, the feed water is reduced linearly to 8.8%
between time = 2 sec and time = 4 sec. Within the same time
the main turbine is by-passed, the pressure of the steam outlet
is reduced linearly from 82.7 bar to 4.0 bar (which is the
inlet pressure to the condenser system), and the free area of
the circulator turbine control valve is reduced to 6.6%. In
fig.16 the sum of the mass flow of all secondary loops has
been plotted and the circulator speed resulting from the
control actions above is shown. The speed of the circulator
in the defective loop is slightly higher because of a
comparatively low energy comsumption as a function of the
circulator mass flow reduced by the leakage mass flow. When the
circulator speed reaches a minimum, it is forced to increase

again and this can be carried out easily by the control system.
Here, the input data are set so as to perform a linear variation
of the blower speeds until it reaches the design value at
time = 100 sec. As a result of these activities four temperatures
in the core are plotted, the uppermost showing the hot-spot
cladding temperature. It can be calculated with constant hot-spot
factors using the second curve which shows the nominal maximum
of an average pin in the central subassembly of the core. As a
result of the control activities and the scram, the cladding
temperatures rise to a maximum at time = 6 sec. This could be
avoided by a slower shut-down of the circulator turbine control
valve but it would lead to greater temperature gradients as well.
The control activities can thus be optimized to minimize the
positive and negative temperature gradients during the first
40 seconds of the accident. Afterwards, the helium density in
the core will be so small that the shut-down heat removal is
reduced and temperatures rise to a maximum at time = 200 sec.
Fig.17 shows the heat transfer parameters of the central
subassembly that can be observed near the interface of the
smooth and rough regions. Two values are plotted for the smooth
region, i.e. Re_S and Nu_S, and two for the rough region, i.e.
h^+ and Nu_R. At first, the Reynolds-numbers fall in the same
way as the mass flow which is a function mainly of the circulator
speed. When this reaches a minimum the gradients of the flow
domains are reduced rapidly but they increase again with
falling helium density. The transition region is already reached
during the first rapid slope. Even when the back-up pressure is
attained in the primary loop and the flow tends towards steady-
state values, we are still very close to the lower boundary of
the transition region. As a result, the Nusselt numbers fall in
the same way as the Reynolds-numbers but the value for the rough
region falls more rapidly than that of the smooth part. For the
design point we gain a factor of 2.4 on the value of the smooth
part by using a two-dimensional roughness, but at time = 200
this factor is only 1.3.

Since the heat transfer parameters have reached steady-state
values after 100 seconds, the temperatures in fig.16 rise
until the driving temperature difference is big enough to
match the shut-down heat removal from the core. They fall
again with the decreasing amount of shut-down heat generated
in the core.

7.2 The first flow-coast-down accident

The series of flow-coast-down accidents is started by a version
with the shut-down rods activated in the same manner as in
chapter 7.1. The 4-link-core version of the computer code is
used (see chapter 6.2). Fig.18 shows the variables as functions
of the time. By contrast with fig. 16, the time starts with
time = 1 sec for the design point, time = 2 sec for the
beginning of the accident when all 8 circulators loose power,
and time = 3 sec for the point of activation of the shut-down
rods. Control activities in the secondary loops are reduced
to a variation of the feed-water mass flow proportional to
the helium mass flow. The minimum feed-water flow is 3.6% of
the design value. The main turbine is not by-passed, but the
outlet pressure of the main turbine control value is reduced
to 3.6 bar. This is no input condition but a result of
calculation following chapter 4.5. Since the volume flow
remains approximately constant, the steam density varies
proportional to the steam mass flow which is, for the first
iteration, the feed-water mass flow. As no control orders act
on the circulator turbine control valve, the densities in the
whole steam loop are reduced considerably. To avoid high
pressure differences across the tubes of the heat exchangers
in such critical situations, the control options might be
changed in order to achieve high pressures in the steam loops.
The circulators loose power by stepwise reduction down to zero
of the circulator turbine power output at time = 2 sec. This
would lead to a stand-still of the shaft but the minimum speed
is supposed to be 300 rpm. The bearings of the shafts are

lubricated by water at tangential velocity, which drives the circulators until the flow of water can no longer be maintained, this probably occurs after 20 minutes. The gradients of the deceleration of the shafts are functions of the moments of inertia. For the loop version with a single-stage steam turbine connected to a single-stage circulator and a design speed of 13000 rpm, the moment of inertia is $6.669 \cdot 10^{-3} kJ \, sec^2$, which is very small. This value could be increased considerably by the use of electric motors connected to multi-stage circulators. Fig.18 shows results for a five-fold value. Besides, some variables are plotted up to time = 50 sec also for the one-fold(b) and ten-fold(a) values. The figure shows the mass flow through the core in percent and in kg/sec, the speed of the shaft, and the pressure which nearly stays constant because no helium gets lost in the primary loops. With respect to the normalized power and the normalized mass flow, the plot shows important differences in the history of the three accidents with different moments of inertia.

For the lower mass flow curve(b) the power is nearly always higher than the capability to remove it, whereas for the upper curves this is not true, at least for the first 230 seconds of the accidents. Consequently, the temperatures of the core vary in much different ways. Three temperatures are plotted, one for the maximum hot spot of the central subassembly, one for the maximum nominal value at that point, and one for the maximum nominal value for an average pin in an average subassembly of the radial blanket. The temperatures of the core inlet and outlet plena of the core are added. The hot-spot temperature is shown for all three different moments of inertia. The uppermost curve(b) rises rapidly immediately after the initiation of the accident because the activation of the shut-down rods is delayed for one second and because the mass flow drops with a time constant less than two seconds. The rest of the curves has a maximum near time = 4 sec and falls to a minimum until the mass flow curve reaches and surpasses the power curve. Here, the back-up speed gained by the water lubrification is a main

parameter and is responsible for the possibility of the
normalized mass flow to fall or not to fall below the value
of the normalized power. The temperatures reach a maximum after
200 seconds because afterwards the shut-down heat still decreases
while the mass flow stays constant. The maximum cladding
temperature in the blanket seems to be unaffected by all those
effects, but this is due to the fact that there are only smooth
surfaces, slightly higher levels of shut-down heat generation
combined with a comparatively high heat capacity of the structure
material, and design point conditions which are very different
from those in the core region. The cladding temperature
distribution along an average pin of the blanket varies but
slightly with the time (the maximum deviation being about
50 Kelvin at one point). The mass flow decreases very similar
to the parallel links of the core, but the heat transfer
coefficient falls much quicker than that in the core region
because, at the design point of the blanket, we are already
near laminar flow (Re $\approx$ 6400). Thus, at time = 5 sec, the heat
transfer coefficient in the core is reduced by 39.5% while the
blanket coefficient is reduced by 74.3%. The blanket coefficent
has reached a quasi-steady state value very soon ($\approx$ 13% of the
design point value), but the core coefficient still decreases
at time = 100 sec where it has reached 3%. The heat capacity
of the blanket, which is high compared with the shut-down heat
generation, flattens the temperature gradients considerably.
The maximum of the cladding temperature in the blanket will
occur beyond time = 300 sec, and thus is not calculated by the
code. Since reduced generation of the blanket is 6% rather
than 3% in the core, the reduced heat transfer coefficient
13% rather than 3%, and the reduced mass flow has nearly the
same value, the maximum cladding temperature in the blanket
should be less than that in the centre of the core.

The core inlet temperature decreases slightly because of the
high efficiency of the heat exchangers at the helium density
of the design point.

7.3 The second flow-coast-down accident

The main differences of the accident treated here as compared to that in chapter 7.2 are the use of the thirteen-link-core (see chapter 6.3) and that the minimum of the blower speed is only 200 rpm. The time scale starts at time = 0 sec, the accident occurs at time = 1 sec and the shut-down rods are activated at time = 2 sec, resulting in a linear variation of the reactivity between time = 2.15 sec and 2.8 sec (see chapter 7.1). Fig.19 shows the power, mass flows and the temperatures as calculated by PHAETON2. As the inertia of the shaft is equivalent to the one-fold value of chapter 7.2 the helium mass flow falls rapidly when the circulators loose power stepwise at time = 1 sec. The mass flows in the secondary loops are reduced proportionally. After scramming the power curve soon reaches the shut-down heat level. Besides, the feedback reactivity variation is plotted, showing a rapid increase after activation of the shut-down rods. This is mainly a function of the Doppler feedback, because with only a small amount of heat generated in the rods the mixed mean pellet temperature falls despite the increase in the cladding temperatures. The same but weaker effect on reactivity is obtained by the void coefficient as the helium density decreases with increasing helium temperatures. After 20 seconds the mixed mean pellet temperatures begin to rise again leading to a negative reactivity gradient. The steep reactivity ramps after 80 seconds are functions of the melting cladding surfaces to be described later on. In analogy to the one-fold-inertia curve of the temperatures in chapter 7.2 the cladding and reactor outlet temperatures rise rapidly because the delayed scram produces more energy in the core than the circulator mass flow is able to remove. The big gradients are reduced considerably when the shut-down-heat level is reached but the speed of the shaft is still too small to produce a sufficient mass flow. So the temperatures rise nearly linearly until the cladding begins to melt. In chapter 7.2 the back-up speed of the circulator due to water lubrification is 300 rpm; here it is only 200 rpm which is only 1.5% of the design value.

At 300 rpm the maximum hot-spot cladding temperature is 1250 K, but here it surpasses the 1900 K-limit (nominal temperature limit 1700 K) where we suppose a failure of the cladding material. The model presently existing calculates cladding temperatures in 141 axial elements according to 141 reactivity worths of the steel cladding (see chapter 4.3). Each of these elements is subdivided into 2 radial elements. If the nominal temperature in the inner radial element is higher than 1700 K, the molten steel cladding is supposed to move downwards, solidifying at the position of that downward element whose temperature is lower than 1700 K. Only the mass of one extra element can be solified at the position of another axial element. This result in a change of reactivity because mass is drawn from a position whose reactivity worth is different from that where the mass is added. The greatest effect is obtained at the interface between positive and negative reactivity worths, i.e. between the core and the axial blanket. Unfortunately, the highest cladding temperatures occur just at the lower part of the core region. The first molten element is the tenth from the bottom in link 7 (see fig.12 $(dk/k)_{7.10} = 2.81239 \times 10^{-5}$). The mass of this element is solified in the element below which has a 10 times lower reactivity worth. Thus nearly the whole $(dk/k)_{7.10}$ comes into effect. The time step between two calculations of the cladding temperatures is 0.1 seconds. In this rough model the molten mass is supposed to move to the next element in this interval without any delay. Fig.19 shows the reactivity ramp due to such severe conditions. Thus the rather steep ramp is a first guess which can only give an idea of the maximum posible reactivity gradient to be introduced as initial conditions of a disassembly code. In fig.19 the cladding temperatures, starting with time = 82 sec, are equivalent to the temperatures of the outer pellet surface, because at the point measured, the cladding material has been totally molten. By this, actual heat transmission by radiation can be taken into account, which affects the temperatures in the subassembly wall. At time = 86.7 sec the first subassembly element is molten just

at the position where the cladding started to melt. Although
this might cause a total drop of that subassembly part which
is suspended on the molten element, these effects cannot be
considered with PHAETON2.

7.4 The third flow-coast-down accident

The thirteen-link-core has been used to calculate effects of
strong natural convection. For this purpose, the steam generator
is_placed on a much higher position than that of a normal
integrated primary loop. Fig. 20 shows the PHAETON2-model used
in these calculations. The centre of the heat sink which is
roughly the centre of the steam generator is raised about 10 m
above the centre of the core. With this configuration one can
exspect a strong natural convection. The inertia of the circulator
shaft is equivalent to the five-fold value of chapter 7.2. The
scram parameters are the same as in chapter 7.3. Fig.21 shows
the main data of the present accident. Until time = 100 sec
the speed of the circulator shaft decreases in a normal way,
then the water lubrification of the shaft is supposed to run
down and the speed is forced to decrease linear down to zero.
As result the helium mass flow shows a normal behaviour during
the first 100 sec, but before the speed reaches zero it reverses
and a natural convection is initiated which leads the mass flow
upwards through the core. This quick flow reversal is a result
of the rather steep circulator speed ramp between time = 100 sec
and time = 115 sec. The circulator runs down so fast that the
pressure being built up in the circulator outlet plenum at the
beginning of the lubrication trip still is bigger than that of
the circulator inlet plenum when the circulator already works
as a throttle valve. The characteristics of a standard throttle
valve is reached when the speed falls down to 60 rpm (see fig.6).
The circulator characteristics have been simplified by neglecting
the stall limit. It should be noted here that the circulator
might run into unstable characteristics at very low speed.

This would induce pulsating mass flows at least near the circulator. The one dimensional code cannot give any answer to the stability questions that arise here. Because of the pressure difference across the circulator at stand-still the flow reversal begins here and leads to flow reversals all over the primary loop. This could only be avoided if the circulator runs down slowly enough without inducing instabilities. Running down too slowly would lead to very low mass flows for a long time. During this time, the temperatures would rise considerably. The circulator speed variation is rather arbitrary after the lubrication trip, but running down so fast is the best way to avoid too high temperatures in the core by admitting flow reversal at the same time. With a hanging core and a downward flow at the design point the present progress of the accident seems to be optimal because the flow reverses in such a way that the local natural convection effects of the core point into the same direction as the global convection of the primary loop. Also the instability effects of the circulators tend towards a flow reversal. Five temperatures are plotted showing the maximum cladding temperatures of the core centre, which is represented by the centre link, the maximum cladding temperature of the innermost radial blanket link, and the temperatures of the core inlet and outlet plena. As the flow reverses, the temperature of the inlet plenum exceeds that of the outlet plenum because the mass flow now leads from the outlet plenum to the inlet plenum. The quasi-steady natural convection mass flow is 3.4% of the design point value, the power level in the core is smaller than 3.4% at time = 200 sec. The maximum cladding temperatures occur at time = 180 sec. The results can be effected by the flow resistance of the loops which should be as low as possible especially outside the core. At time = 180 sec the flow domain is at the lower end of the transition region and the cladding roughness is still effective producing a roughness multiplication factor for the Nusselt number of about 1.18. It is clear that at slightly higher flow resistances in the loop, the roughness is of no help any more.

8. Conclusion

For predisassembly accidents of GCFRs the PHAETON2 computer
code has been proved practicable and most accurate. Questions
about computanional methods only arise where design data are
not available and must be supplied by theoretical assumption
(such as pressure drop coefficients in the channels outside
the reactor, circulator characteristics at low speed). As
natural convection is one of the topics in calculating the
shut-down heat removal of GCFRs, it should be noted that global
convection phenomena can be calculated accurately, but local
effects cannot be considered by a one-dimensional model. The
analyses of the dynamics with only natural convection as the
driving force require high precision. In such cases the system
is very sensitive to disturbances so that misleading boundary
conditions, such as the mass flow generation of a running-down
circulator, can produce unrealistic results. For most other
cases there are no such problems.

Looking at the depressurization accident with scram, the back-up
pressure has proved to be most important. Whilst the history
of the beginning of the accident can be changed considerably
by the control system available, the problematic temperatures
occur beyond a time interval of 6 time constants, beginning with
the start of the accident (one time constant of a depressurization
accident is defined to be that time interval during which the
helium pressure is reduced to 37%). To limit the maximum
cladding temperatures well below the point of failure (1700 K
nominal), 2% of the design pressure should be available as a
back-up. For this value the maximum cladding temperature
calculated could possibly vary considerably between two similar
reactors. This is caused by the flow condition in the core which
is always near the interface between laminar flow and the
transition region. In the present case, the flow stays in the
transition region which leads to rather favorablé heat transfer
coefficients.

For the flow-coast-down accidents the inertia of the circulator
shaft has proved to be most important. The first 50 seconds of
an accident can be totally different as a function of a
variation of inertia. For most accidents we can assume that
there is still water available to lubricate the shaft so that
for the first 20 minutes of such an accident we can rely on a
back-up velocity of the shaft. The value of this velocity
determines the second part of the accident with a second maximum
of cladding temperatures. The value of 200 rpm is not sufficient
for the present reactor, but with 300 rpm the maximum temperatures
are well below the point of failure.

Looking at a flow-coast-down accident without any circulator
back-up velocity but with an increased effect of natural
convection, we state that the heat sink of a primary loop
must be raised substantially above the heat source of the
reactor to produce mass flows which are able to remove the
shut-down heat sufficiently.

References

/1/ Bittermann, Goetzmann, Hassmann et al.
1000 MWe GCFR, Jahresbericht 1973-1976, unpublished

/2/ C.A. Goetzmann, M. Dalle Donne
Design and Safety Studies for a 1000 MWe Gas Cooled Fast
Reactor, ANS Fast Reactor Safety Meeting, Beverly Hills,
April 1975, CONF/740401-P2

/3/ D. Wilhelm
Untersuchungen des Störfallverhaltens des GCFR von
1000 MWe mit dem digitalen Rechenprogramm PHAETON2,
Gesellschaft für Kernforschung, Karlsruhe, KFK 1276/3,
1976

/4/ H. Kawamura
Transient Hydraulics and Heat Transfer in a Turbulent
Flow,
Gesellschaft für Kernforschung, Karlsruhe, KFK 2166, 1975

/5/ A. Schwartz
Generalized Reactor Kinetics Code, AIREK II,
NAA-SR-MEMO 4980, February 1960

/6/ Gulf General Atomic
Reference Design of a 1000 MWe Gas Cooled Fast Reactor
Plant, Gulf-GAE-37, Zürich, March 1968

/7/ W. Höbel
Numerical methods used in the two-dimensional neutron
diffusion program DIXI,
Advanced Publications Ltd., London,
to be published as a contribution to a monography

/8/ K. Bauerfeind
Die Berechnung des Übertragungsverhaltens von Turbo-
Strahltriebwerken unter Berücksichtigung des insta-
tionären Verhaltens der Komponenten, Luftfahrttechnik-
Raumfahrttechnik, Vol.14, No.5, May 1968, page 117

/9/ General Atomic, San Diego
privat communication 12-6-1974

/10/ W. Traupel
      Thermische Turbomaschinen, Vol. 1&2, Berlin/Heidelberg/
      New York, 1966, 1968

/11/ K. Rehme
      Laminarströmung in Stabbündeln, Chemie-Ingenieur-Technik
      43, No. 17, 1971

/12/ K. Rehme
      Pressure Drop Performance of Rod Bundles in Hexagonal
      Arrangements,
      Int. J. Heat Mass Transfer, Vol.15, Page 2499, 1972

/13/ M. Dalle Donne, E. Meerwald
      Heat Transfer and Friction Correlations for Surfaces
      Roughened by Transversal Ribs, NEA Core Performance
      Specialist Meeting, Studsvik, 20-6-1973

/14/ M. Dalle Donne, L. Meyer
      Turbulent Convective Heat Transfer from Rough Surfaces
      with Two-dimensional Rectangular Ribs, Int. J. Heat
      Mass Transfer, Vol.20, Page 583, 1977

/15/ M. Dalle Donne
      private communication 15-2-1977

/16/ E.M. Sparrow
      Heat Transfer to Longitudinal Laminar Flow between
      Cylinders, Trans. of the ASME, Series C,Vol. 83,1961,page 415.

/17/ A. Martelli
      Thermo- und fluiddynamische Analyse von gasgekühlten
      Brennelementbündeln,
      Gesellschaft für Kernforschung, Karlsruhe, KFK 2436,
      EUR 5508d, 1977

/18/ Gröber, Erk, Grigull
      Grundgesetze der Wärmeübertragung, Berlin/Göttingen/
      Heidelberg, 1963

/19/ VDI-Wärmeatlas, Verlag des Vereins Deutscher Ingenieure,
      Düsseldorf 1957

/20/ W. Fritz
Grundlagen der Wärmeübertragung bei Verdampfen von
Flüssigkeiten, Chemie-Ingenieur-Technik 35, No.11,
November 1963, page 753

/21/ T.A. Porsching, J.H. Murphy, J.A. Redfield
Stable Numerical Integration of Conservation Equations
for Hydraulic Networks, Nuclear Science and Engineering,
Vol.43, 1971, page 218

/22/ H. Kawamura, K. Torikai
Analysis of Transient Thermo-Hydraulics with a Two-Equation
Model of Turbulence, NEA Specialist Meeting on GCFR Heat
Transfer, Karlsruhe, October 1977

Nomenclature

a	thermal diffusivity (m^2/sec)	
C	blackbody constant	
c	specific heat capacity $(kJ/(kg\ K))$	
c_p	specific heat capacity at constant volume	$(kJ/(kg\ K))$
c_v	specific heat capacity at constant pressure	$(kJ/(kg\ K))$
c_i	concentration of the precursors of group i	
d_h	hydraulic diameter (m)	
d_s	pin diameter (m)	
$\vec{f}$	vector function	
F	cross section area (m^2)	
g	gravitational acceleration $(9.81\ m/sec^2)$	
$G(h^+)$	heat transfer function of the roughness	
h^+	non-dimensional roughness height	
h_R	roughness height (m)	
i	enthalpy (kJ/kg)	
k	effective multiplication factor	
k_w	thermal conductivity $(kW/(m\ K))$	
K_A	axial expansion reactivity constant	
K_D	Doppler reactivity constant	
K_R	radial expansion reactivity constant	
K_H	helium density reactivity constant	
K_v	friction force per volume (kJ/m^4)	
l	effective life-time of the prompt neutrons	
m	mass flow (kg/sec)	
M	momentum (kJ)	
N	power (kW)	
Nu	Nusselt number	
p	pressure (kJ/m^3)	
P_s	pitch of the pins in hexagonal arrangement (m)	
Pr	Prandtl number	
$\dot{p}$	pressure ramp dp/dt $(kJ/(m^3\ sec))$	
q	heat flux (kW/m^2)	
q_v	power per fluid volume (kW/m^3)	
r	radial distance (m)	
R	gas constant $(kJ/(kg\ K))$	
R_w	thermal resistance fluid-wall $(m\ K/kW)$	
Re	Reynolds number	

$R(h^+)$ friction function of the roughness

t   time   (sec)

T   absolut temperature   (K)

T^* temperature see page 32   (K)

$\dot{T}$ temperature ramp   (K/sec)

u   internal energy   (kJ/kg)

V   volume (m^3)

$\dot{V}$ volume flow (m^3/sec)

w' velocity   (m/sec)

x   axial distance   (m)

$\vec{y}$ vector of state

Z   speed of the shaft   (1/sec)

α   heat transfer coefficient $(kW/(m^2\ K))$

β   effective part of delayed neutrons

γ   angle of the axis in respect to the horizon

Δ   step interval

ε   radiation emissivity

ζ   drag coefficient

η   dynamic viscosity   (kg/(m sec))

θ   mass momentum of inertia $(kJ\ sec^2)$

λ   Weisbach friction factor, decay constant

ν   number of neutrons

ρ   density (kg/m^3)

ρ_ν reactivity

ω   angular velocity   (1/sec)

ω_R heat transfer parameter in a helium node, page 30 (1/sec)

ω_D heat transfer parameter in a steam node, page 33
        (kW/(kg K))

Subscripts

A   exit

E   entrance

i   i-th node, i-th element, i-th group

L   Last time step

st   steady state

tr   transient
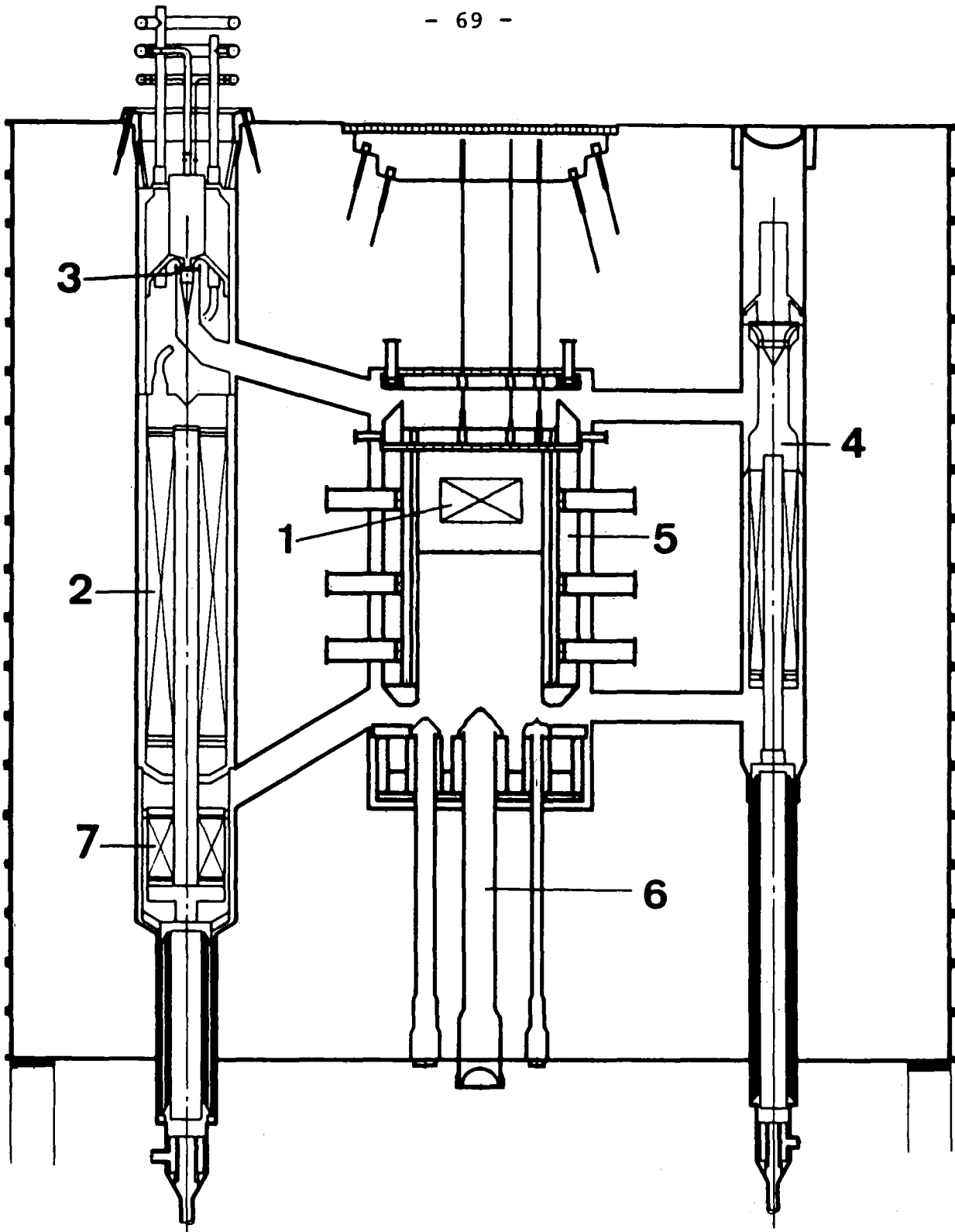
1 Reactor Core   5 Radiation Shield
2 Steam Generator   6 Fuel Handling Penetration
3 Helium Circulator   7 Resuperheater
4 Auxiliary Loop

Fig.1   Cross section through the PCRV of the
1ooo MWe reactor from ref./1/ and /2/
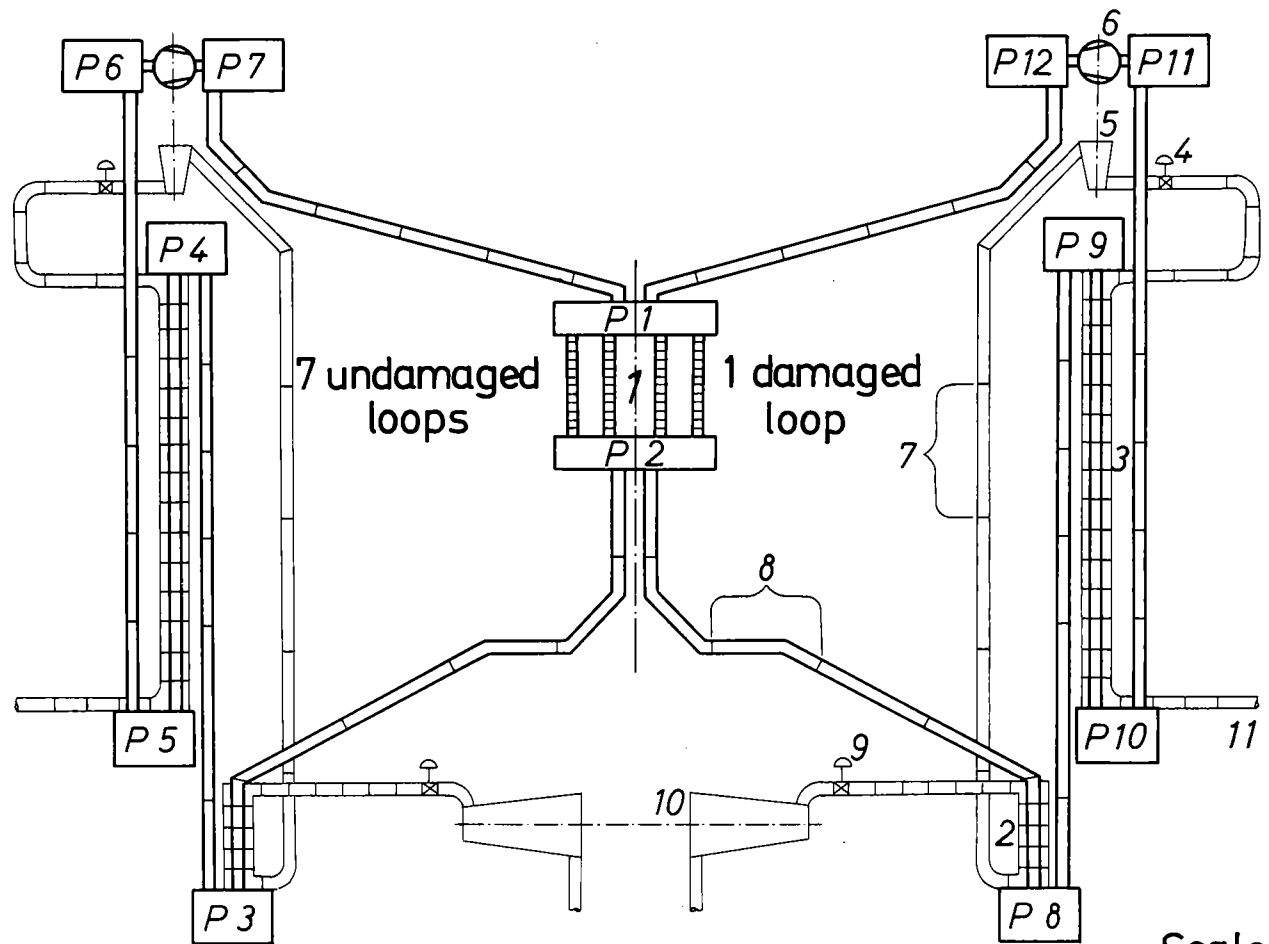
7 undamaged loops

1 damaged loop

1 Reactor
2 Resuperheater
3 Steam Generator
4 Circulator Turbine Control Valve
5 Circulator Turbine
6 Helium Circulator

7 Node of Steam Loop
8 Node of Helium Loop
9 Main Turbine Control Valve
1o Main Steam Turbine
11 Feedwater Inlet

P1 - P12 Plenum of Helium Loop

Scale
1m

Fig.2 PHAETON2-model of the 1ooo MWe reactor with 4 core links
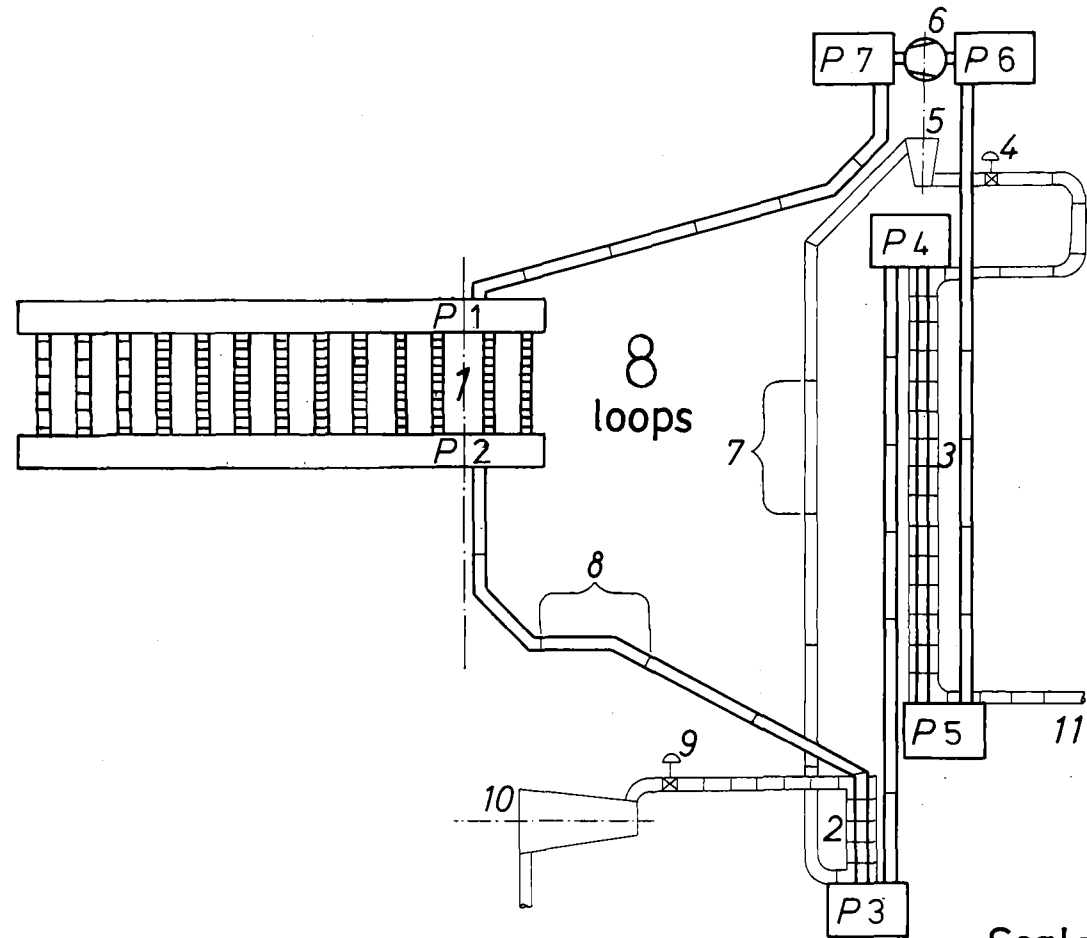
1 Reactor
2 Resuperheater
3 Steam Generator
4 Circulator Turbine Control Valve
5 Circulator Turbine
6 Helium Circulator

7 Node of Steam Loop
8 Node of Helium Loop
9 Main Turbine Control Valve
1o Main Steam Turbine
11 Feedwater Inlet

P1 - P7   Plenum of Helium Loop

Fig.3   PHAETON2-model of the 1ooo MWe reactor with 13 core links
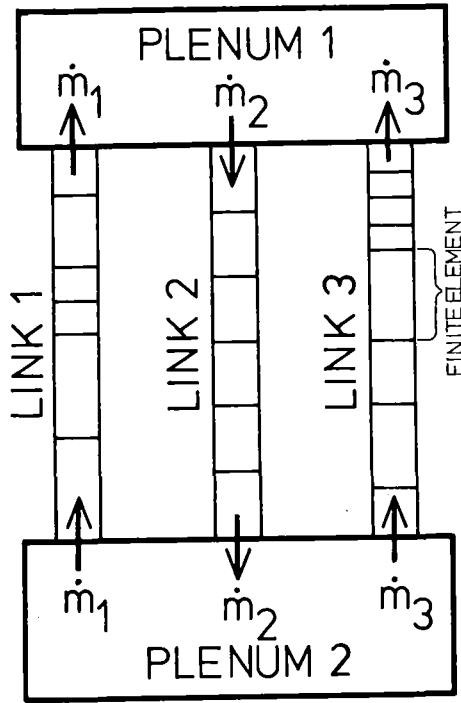
Fig.4 Simplified model of a helium loop
with 2 plena and 3 links
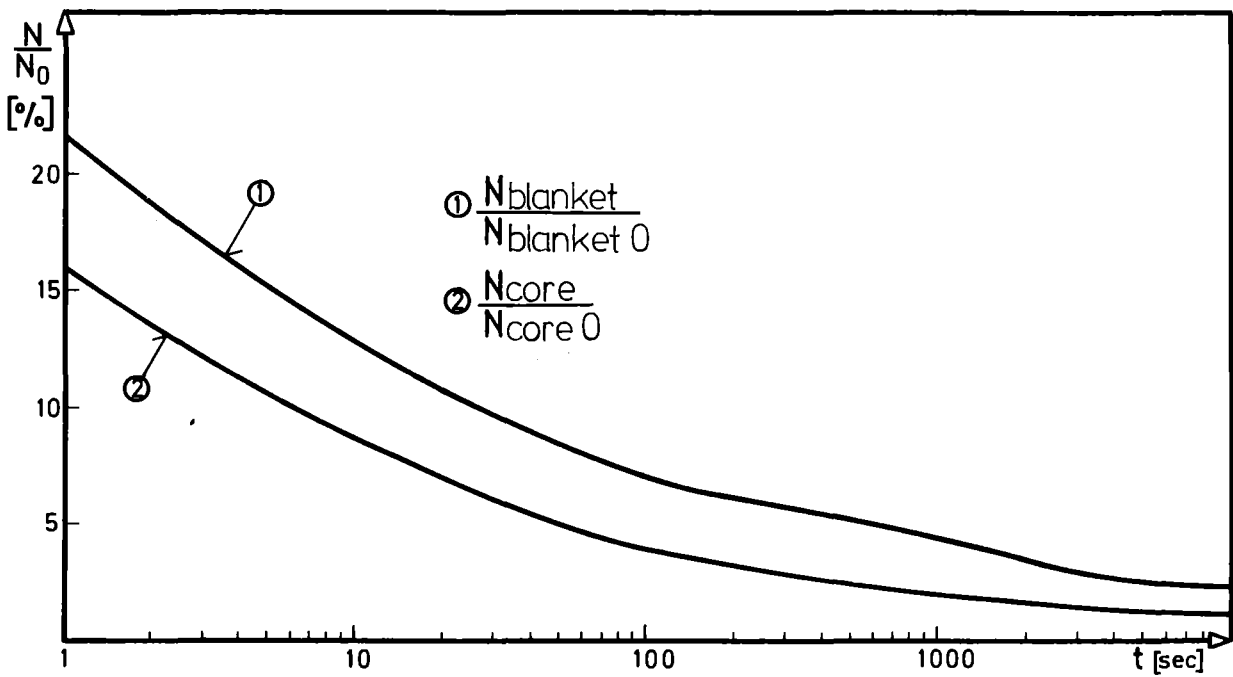
Fig.5 Decay heat variation with time
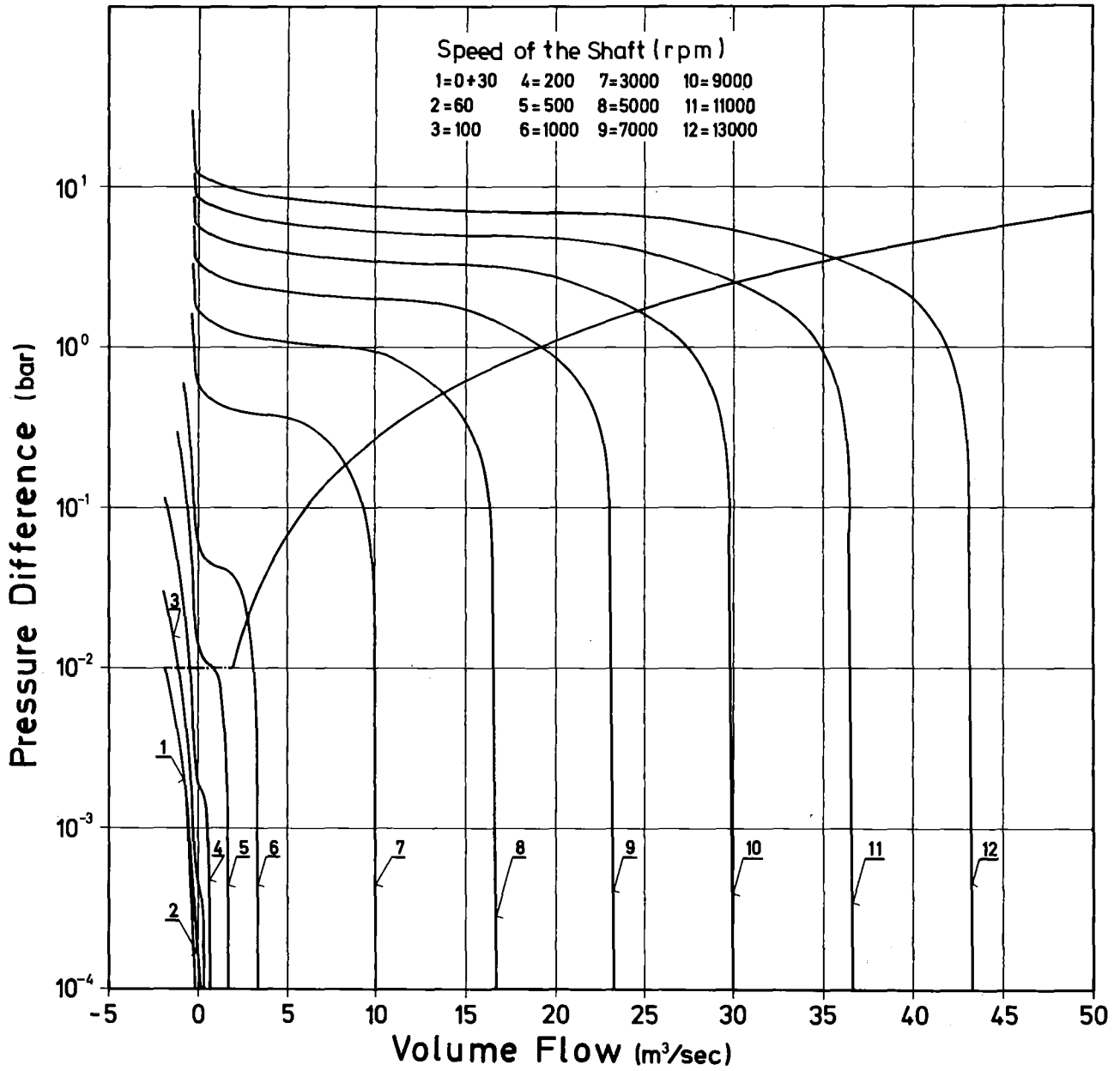
Fig.6   Helium circulator characteristics
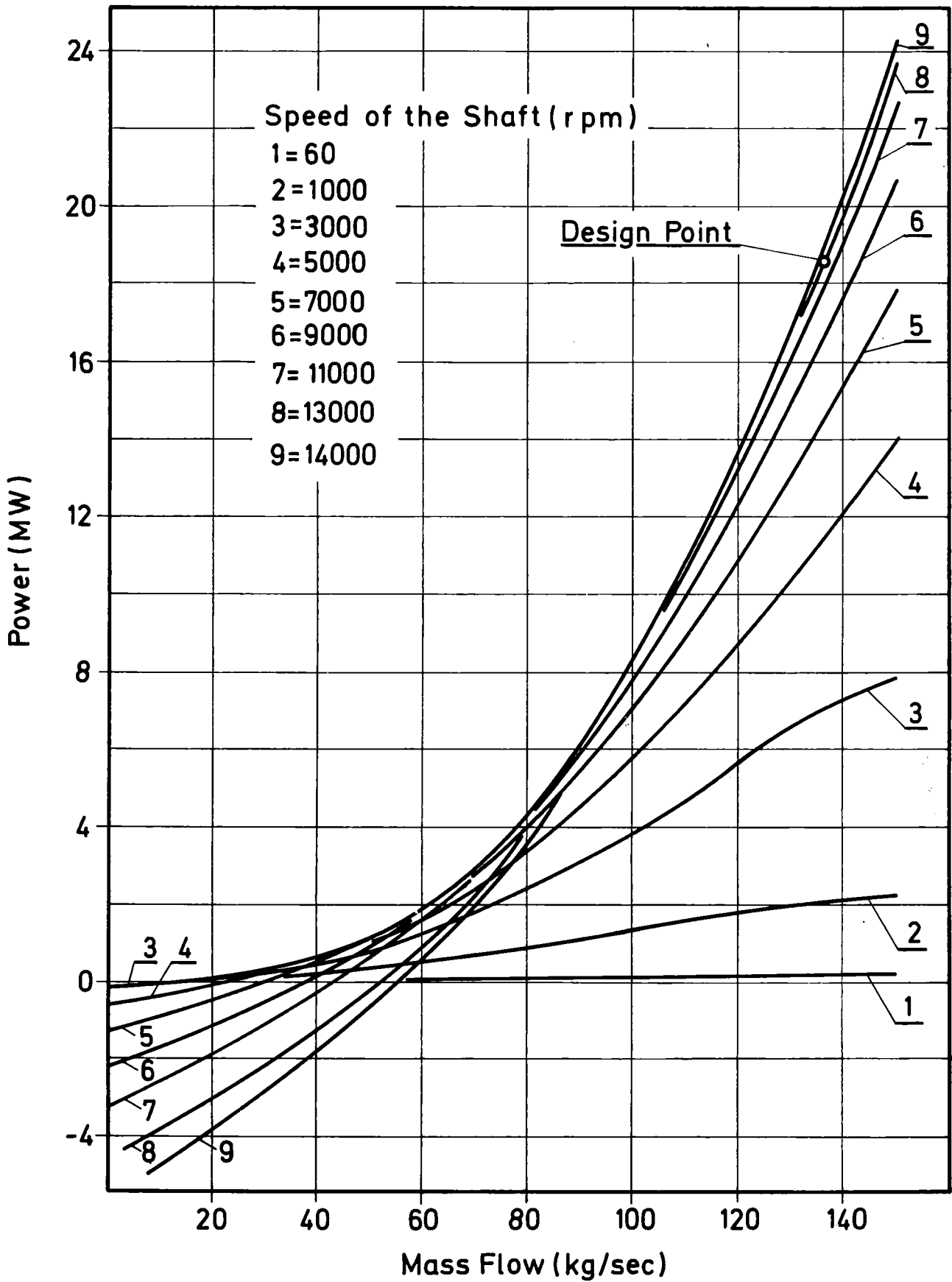
Fig.7 Circulator turbine characteristics
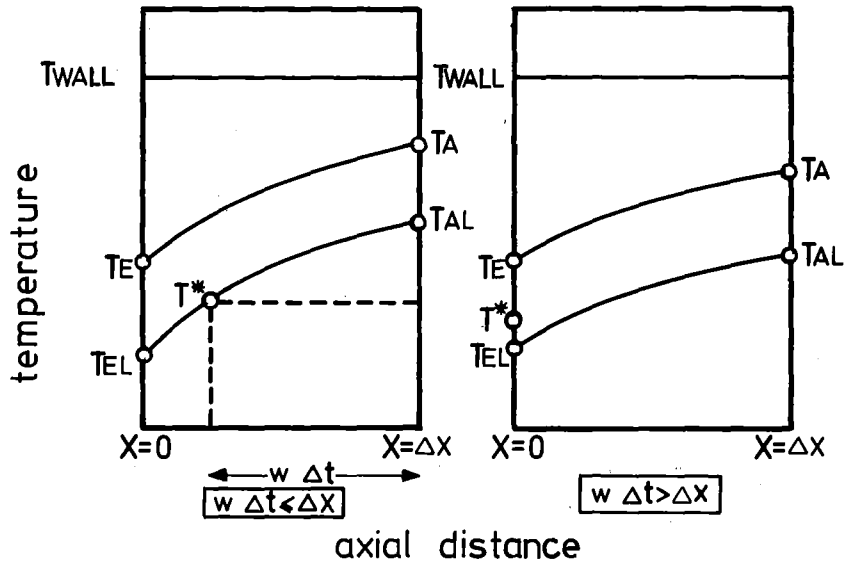
Fig.8 Definition of the helium node temperature T*

SCEME OF THE MATRIX FOR THE HYDRAULIC NETWORK
THE X- AND *-ELEMENTS ARE NON-ZERO
THE *-ELEMENTS FORM THE MAIN DIAGONAL

Fig.9 Matrix of the hydraulic network
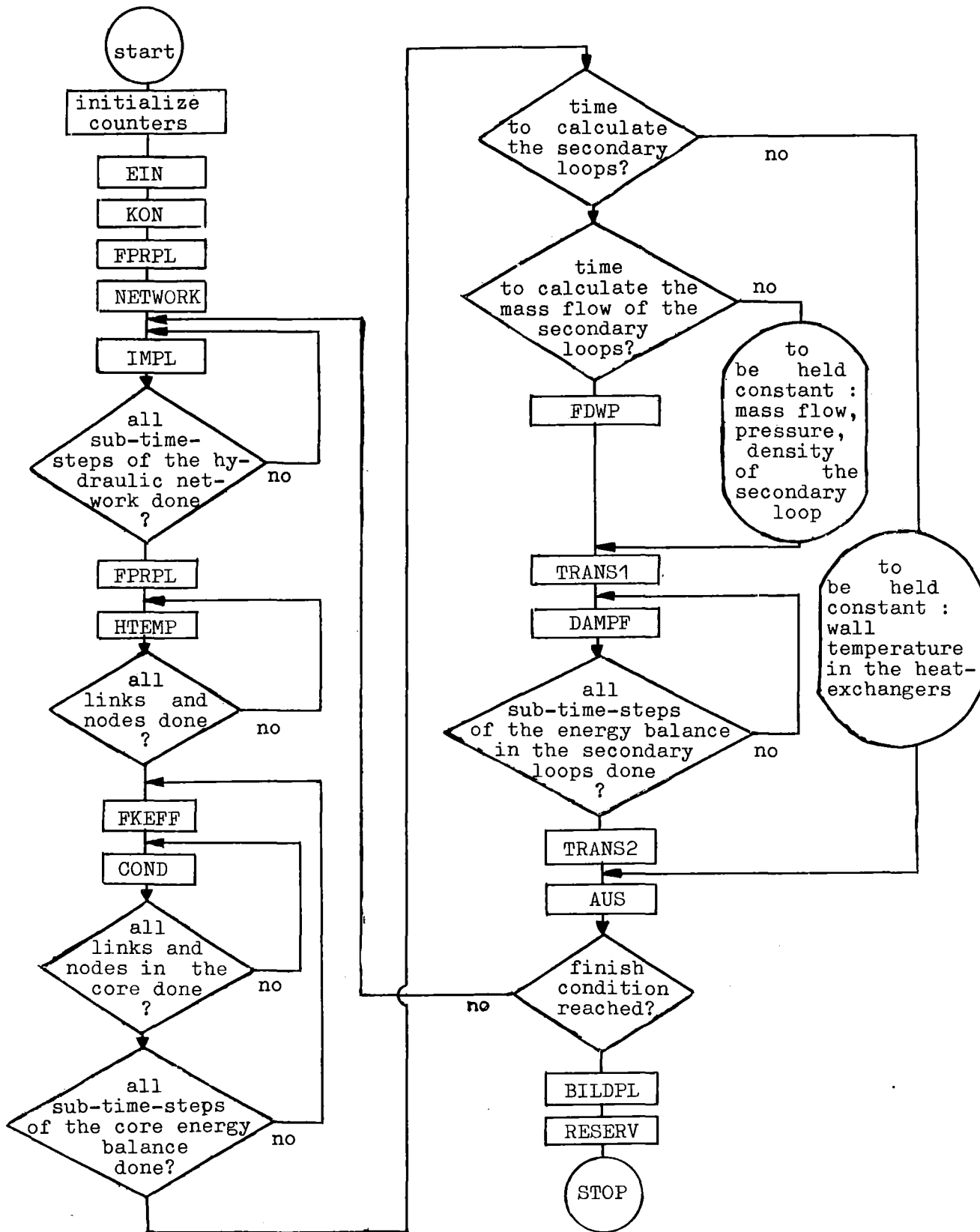
Fig.1o   Simplified flow chart of the main program
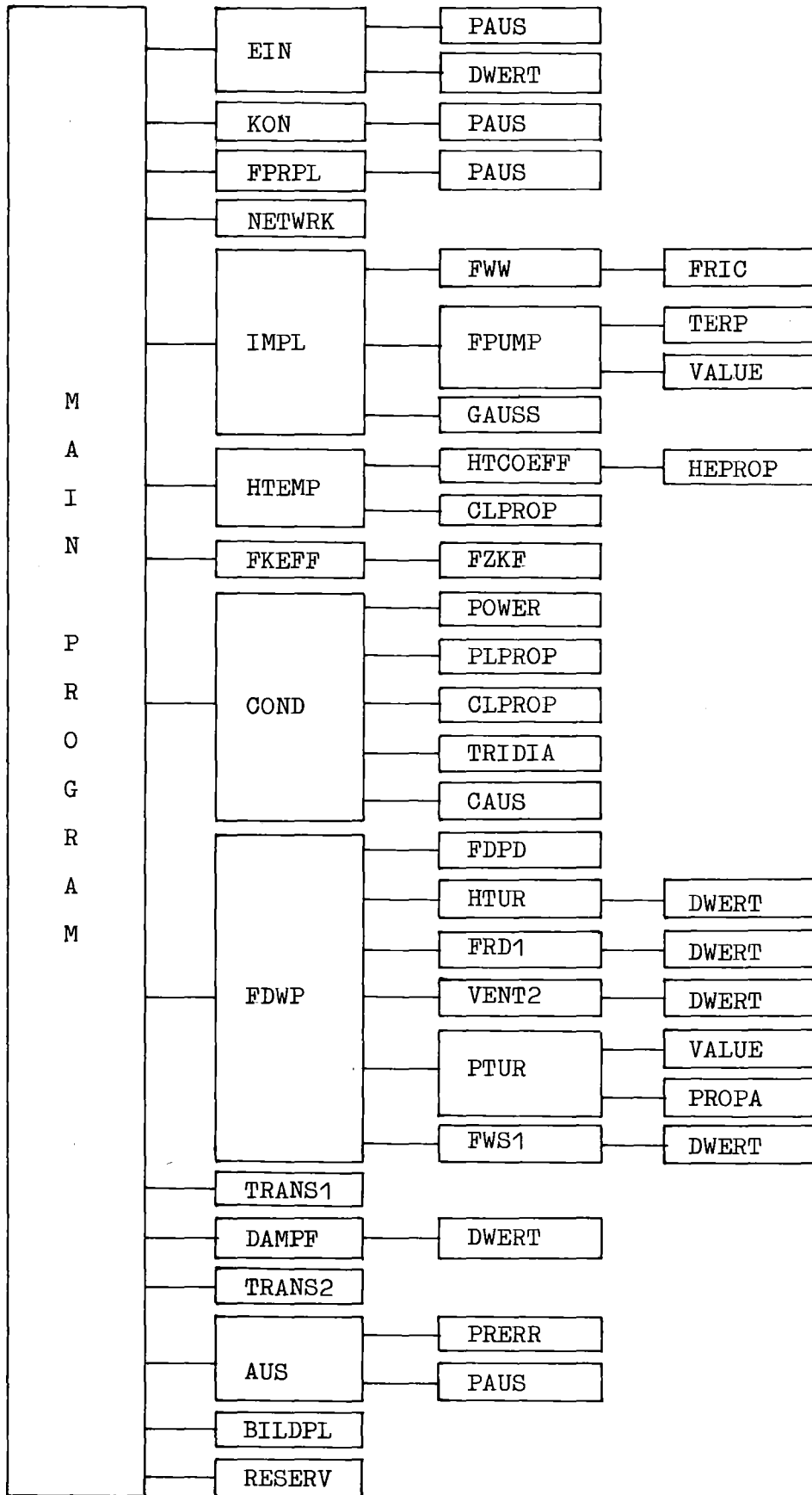
Fig.11 Sceme of the subroutines in PHAETON2

REAKTIVITY DK/K CAUSED BY A TOTAL LOSS OF STEEL CLADDING

LINK-NR.

7	8	9	10	11	12	13	14	15	16
-6.71556E-06	-4.01551E-05	-7.96399E-05	-1.18168E-04	-1.18011E-04	-1.93568E-04	-1.51736E-04	-2.57726E-04	-1.60664E-04	-1.88424E-04
2.89818E-06	1.72004E-05	3.32811E-05	4.60814E-05	3.90820E-05	3.94907E-05	9.99008E-06	-5.53405E-05	-8.74656E-05	-2.35599E-04
2.80553E-05	1.67439E-04	3.29670E-04	4.79382E-04	4.58476E-04	6.83810E-04	4.73422E-04	5.99456E-04	2.10992E-04	-1.24259E-04
5.53808E-05	3.30618E-04	6.51920E-04	9.51722E-04	9.16749E-04	1.38858E-03	9.81901E-04	1.31789E-03	5.37585E-04	-2.91201E-06
7.82354E-05	4.67174E-04	9.21790E-04	1.34762E-03	1.30104E-03	1.98023E-03	1.40897E-03	1.92104E-03	8.11465E-04	9.89536E-05
9.12057E-05	5.44582E-04	1.07498E-03	1.57234E-03	1.51937E-03	2.31639E-03	1.65165E-03	2.26366E-03	9.67021E-04	1.56918E-04
9.12251E-05	5.44668E-04	1.07523E-03	1.57274E-03	1.51972E-03	2.31698E-03	1.65209E-03	2.26415E-03	9.67263E-04	1.56950E-04
7.82868E-05	4.67486E-04	9.22417E-04	1.34850E-03	1.30199E-03	1.98159E-03	1.40998E-03	1.92248E-03	8.12123E-04	9.92697E-05
5.54504E-05	3.31037E-04	6.52690E-04	9.52905E-04	9.17921E-04	1.39045E-03	9.83273E-04	1.31984E-03	5.38471E-04	-2.59699E-06
2.81239E-05	1.67935E-04	3.30456E-04	4.80504E-04	4.59591E-04	6.85551E-04	4.74673E-04	6.01313E-04	2.11872E-04	-1.23980E-04
2.94167E-06	1.74594E-05	3.37986E-05	4.68353E-05	3.98094E-05	4.04908E-05	1.07990E-05	-5.41818E-05	-8.6916CE-05	-2.35399E-04
-6.67655E-06	-3.99644E-05	-7.92369E-05	-1.17474E-04	-1.17349E-04	-1.92508E-04	-1.50921E-04	-2.56428E-04	-1.59866E-04	-1.87493E-04

LINK-NR.

17	18	19
-4.84816E-05	-6.00966E-06	-7.22222E-07
-2.96167E-04	-3.45053E-05	-3.77270E-06
-5.76507E-04	-7.38783E-05	-8.45436E-06
-7.03873E-04	-9.17425E-05	-1.06525E-05
-5.76860E-04	-7.39295E-05	-8.46046E-06
-2.96721E-04	-3.45661E-05	-3.77848E-06
-4.82331E-05	-5.99134E-06	-7.20496E-07

EACH VALUE IS AN AVERAGE IN A NODE FORMED BY THE PHAETON2-MODEL.
LINK 7 TO 16 REPRESENT CORE LINKS WITH 1 NODE FOR THE UPPER AND LOWER AXIAL
BLANKET AND 10 NODES FOR THE CORE REGION INBETWEEN. LINK 17 TO 19 REPRESENT
LINKS OF THE RADIAL BLANKET WITH THE UPPERMOST AND LOWERMOST NODES OF THE
SAME SIZE AS IN THE CORE REGION. THE 5 NODES INBETWEEN ARE TWICE AS LONG AS
THOSE IN THE CORE REGION.

Fig.12   Steel cladding reactivity worths

Subassembly characteristics

(first value: core subassembly, second value: blanket subass.)

number of subassemblies in the inner core region	85
number of subassemblies in the outer core region	108
number of subassemblies in the radial blanket region	180
thickness of the hexagonal subassembly wall	4mm
spanner width of the subassembly wall	189mm
number of pins in a subassembly	271/169
diameter of the pin	8.2mm/13.1mm
pitch of the pins in hexagonal arrangement	11mm/13.7mm
hydraulic diameter	7.79mm/3.37mm
radius of the zero-shear-stress line of the equivalent annulus	5.78mm/7.19mm
diameter of the pellet	7.14mm/11.9mm
thickness of the steel cladding	.53mm/.6mm
Nusselt number of the fully develloped laminar flow	9.54/2.7
Weisbach friction factor of the laminar flow multiplied by the Reynolds number	27.63/15.76
length of the smooth section of the cladding	444.3mm/1481mm
length of the rough section of the cladding	1036.7mm/.0mm
length of the upper and lower axial blanket (smooth surface)	600mm
height of the rectangular two-dimensional roughness	.1mm
width of the rectangular two-dimensional roughness	.1mm
pitch of the rectangular two-dimensional roughness	.7mm

Reactivity values

reactivity constant of axial expansion	$K_A = -2.27 \times 10^{-6}$
reactivity constant of radial expansion	$K_R = -7.47 \times 10^{-6}$
reactivity constant of helium density variation	$K_V = -4.471 \times 10^{-3}$
Doppler reactivity	$\frac{1}{k}\frac{\partial k}{\partial T} = .082 \, T^{-3/2} - .008 \, T^{-1}$

weighting factors for the Doppler feedback:

inner core region	.4939
outer core region	.2250
total blanket	.2811

Design point characteristics

maximum linear power in the core centre	42.9 kW/m
axial form factor	1.25
radial form factor	1.09
thermal power of the core and the blanket	2779 MW
thermal power of the core	2644 MW
power of all helium circulators	148 MW
helium inventory	10156 kg
maximum helium pressure	120 bar
total pressure drop of a loop with the core	6 bar
pressure drop in the core	5 bar
total helium flow through the core	1868 kg/sec
core inlet helium temperature	547 K
mixed medium core outlet temperature	832 K
total steam flow through the heat exchangers	1088 kg/sec
feedwater pressure	209 bar
feedwater temperature	443 K
hot spot factor of the helium temperature difference	1.17
hot spot factor of the heat transfer fluid-wall	1.39
hot spot factor of the heat generation in the pellet	1.17

Constant properties

specific heat capacity of helium	5.22 kJ/(kg K)
ratio of specific heat of helium	1.667
Prandtl number of helium	0.667
gas constant of helium	2.078 kJ/(kg K)
density of the pellets	9113.4 kg/m³
density of steel (cladding, subassembly wall)	8000 kg/m³
thermal conductivity of the pellets	1.9×10^{-2} kW/(m K)
thermal conductivity of steel	2.284×10^{-2} kW/(m K)
specific heat capacity of the pellets	.3349 kJ/(kg K)
specific heat capacity of steel	.5862 kJ/(kg K)

Fig.13   Main data of the 1000 MWe reactor
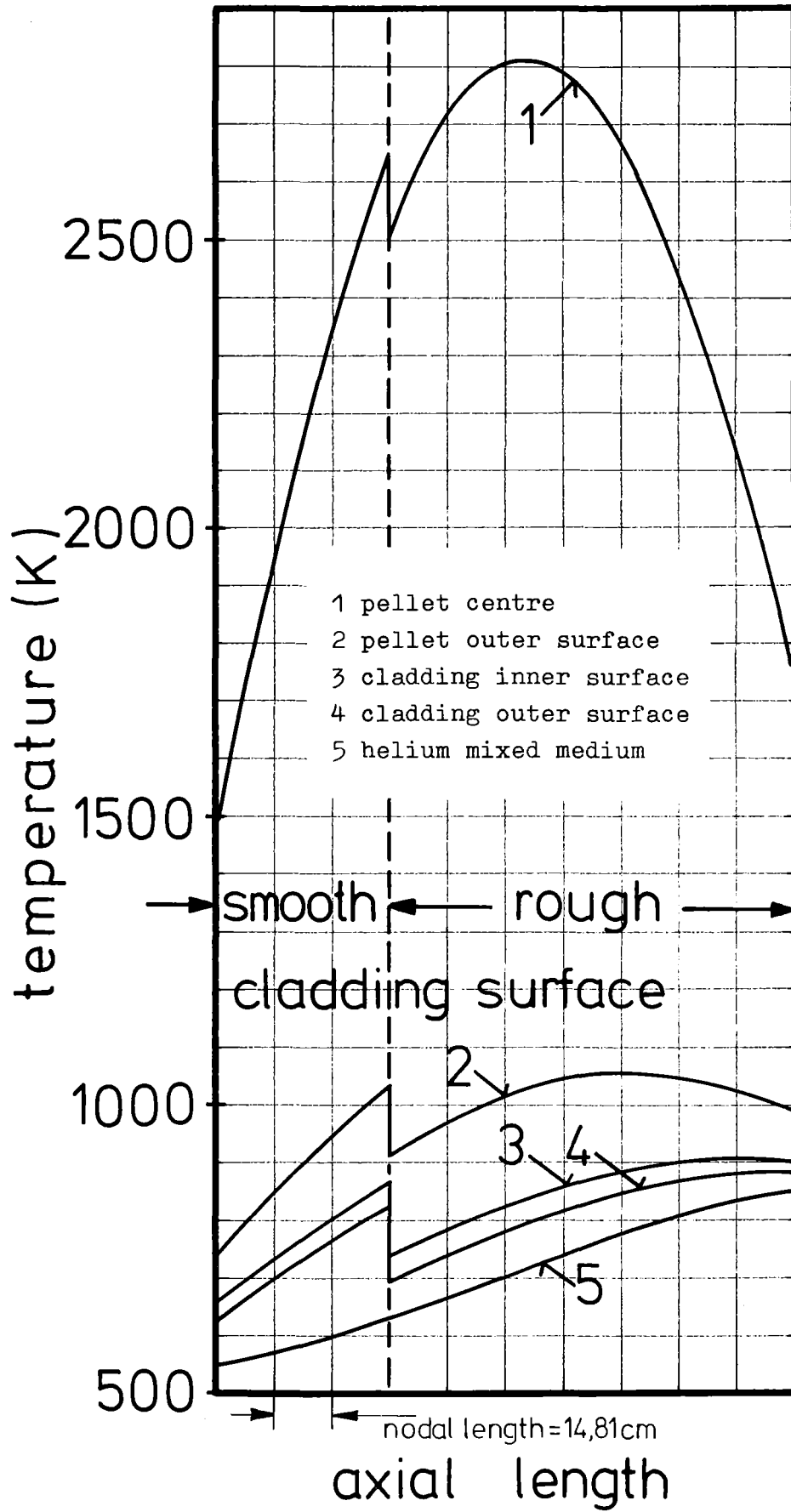
Fig.14   Temperatures of an average pin in the
central subassembly at the design point
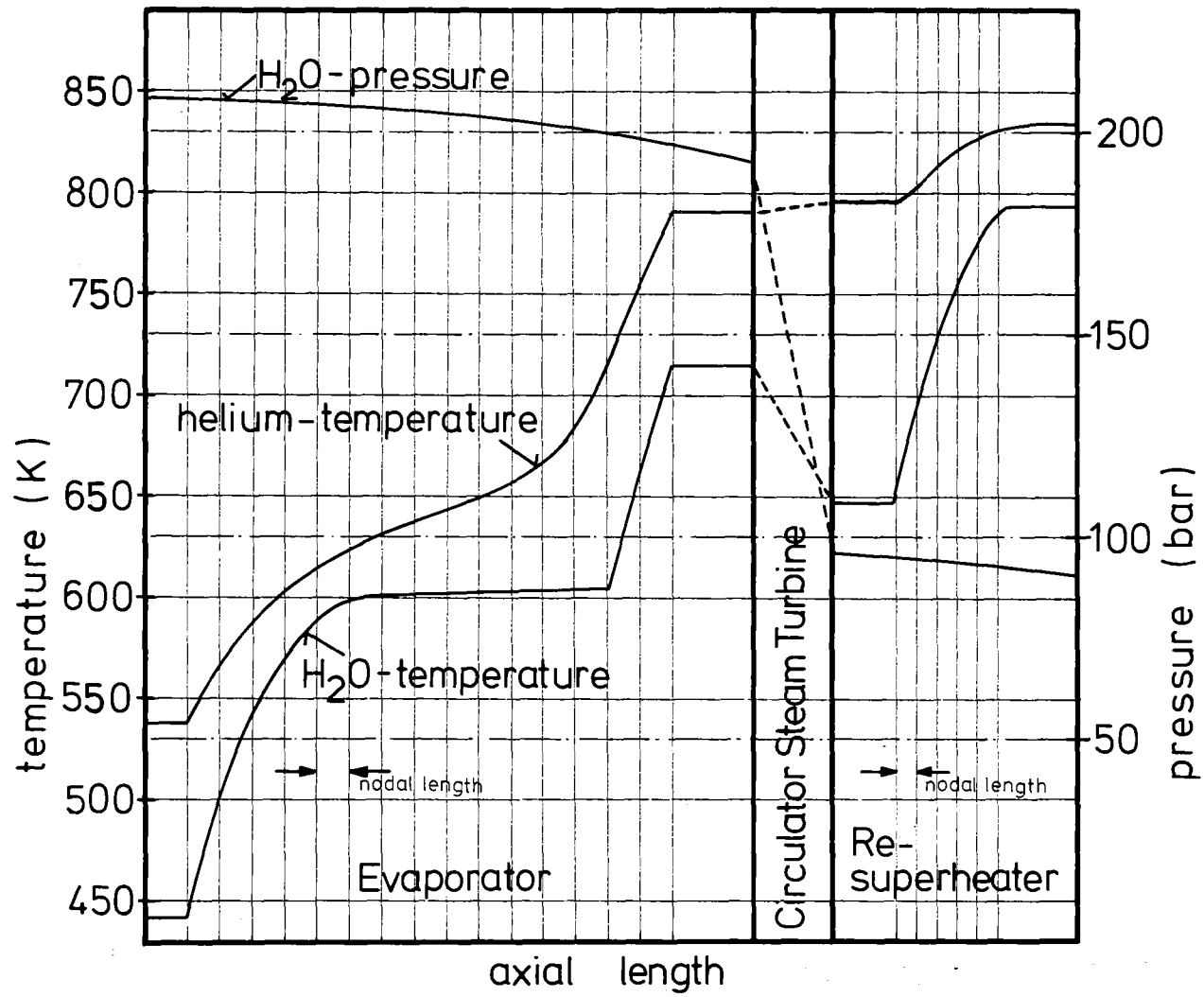
Fig.15   Temperature and pressure distribution in the heat exchangers
at the design point
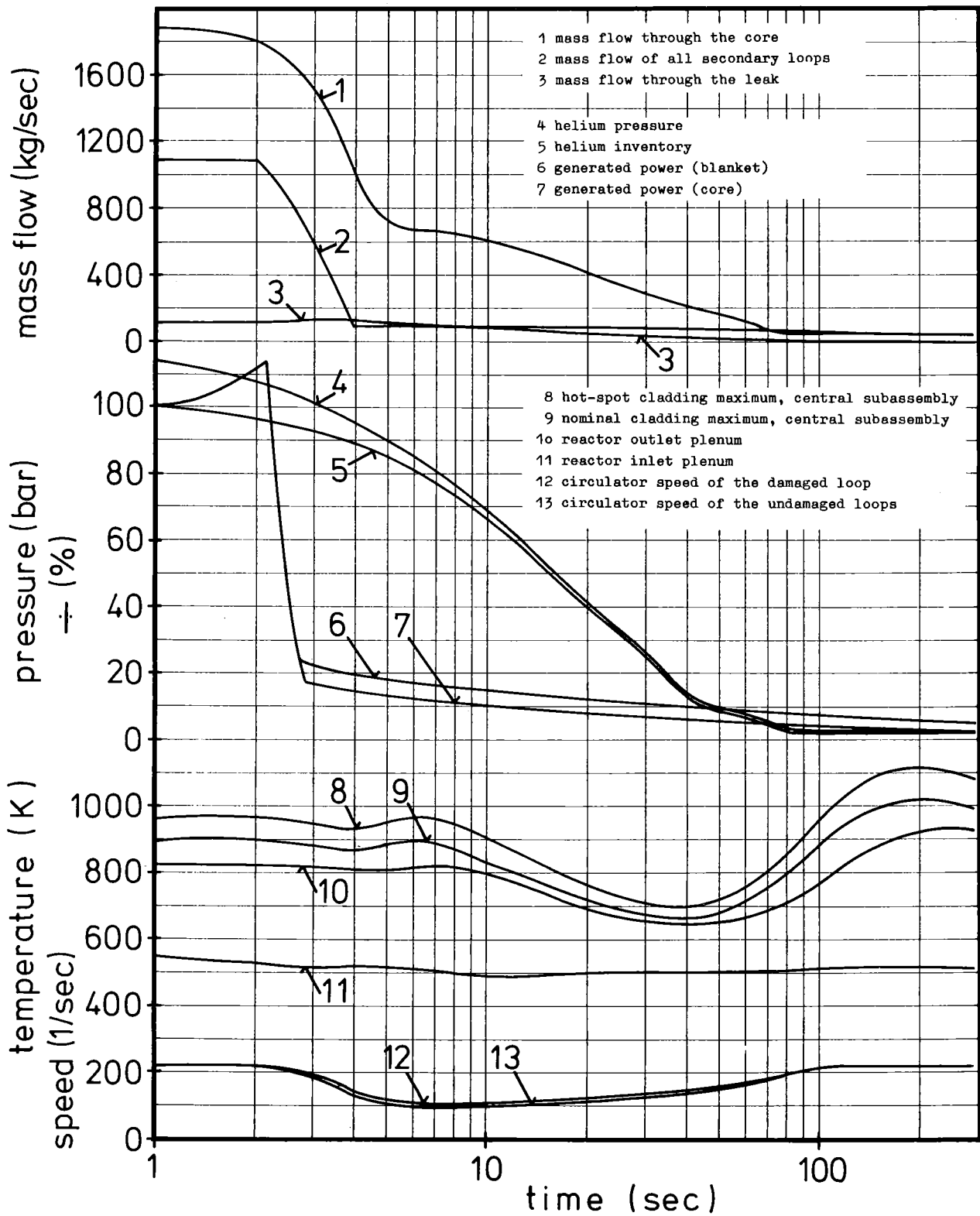
Fig.16 The main output of the depressurisation accident
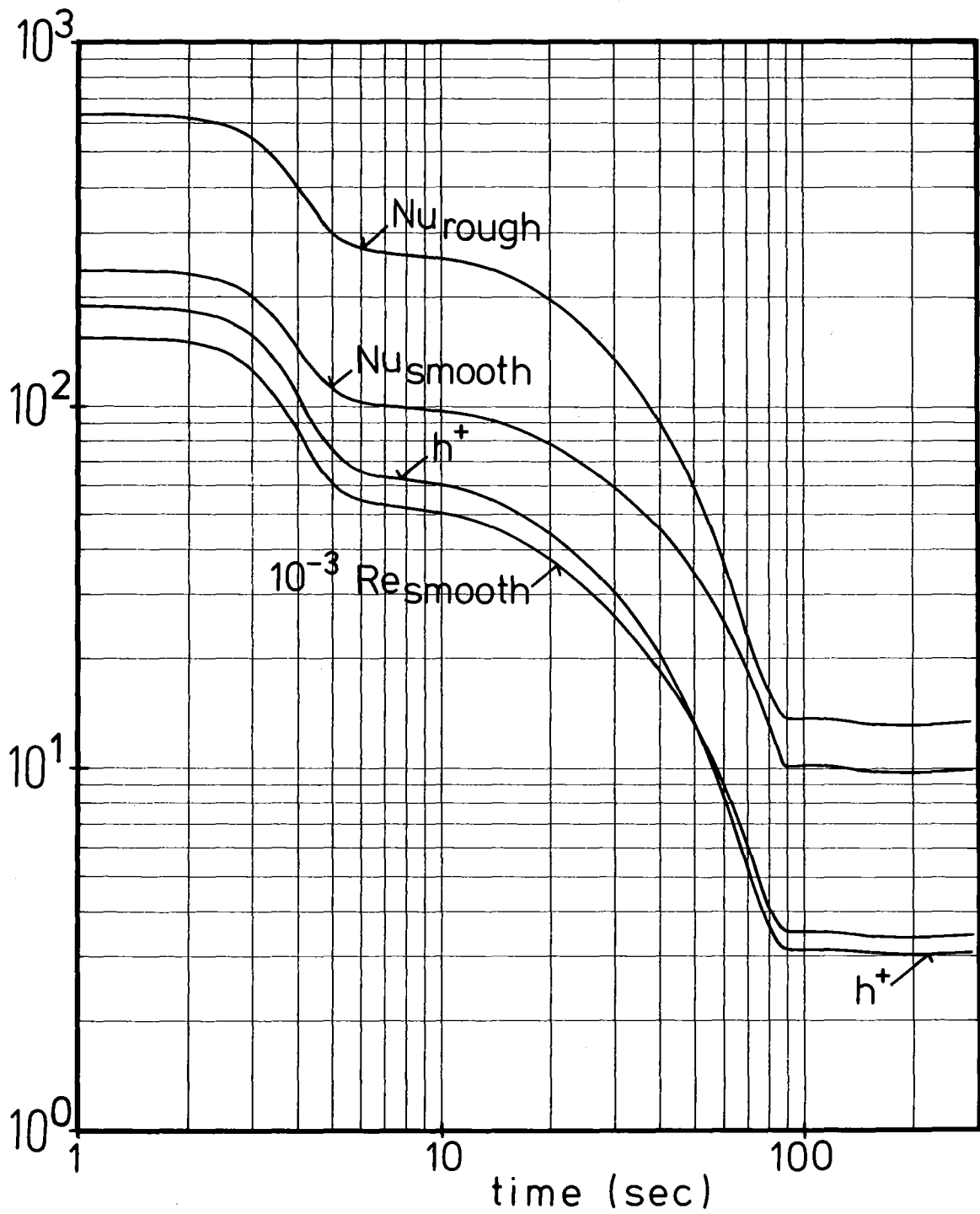
Fig.17 The heat transfer parameters of the
depressurisation accident

FLOW-COAST-DOWN ACCIDENT
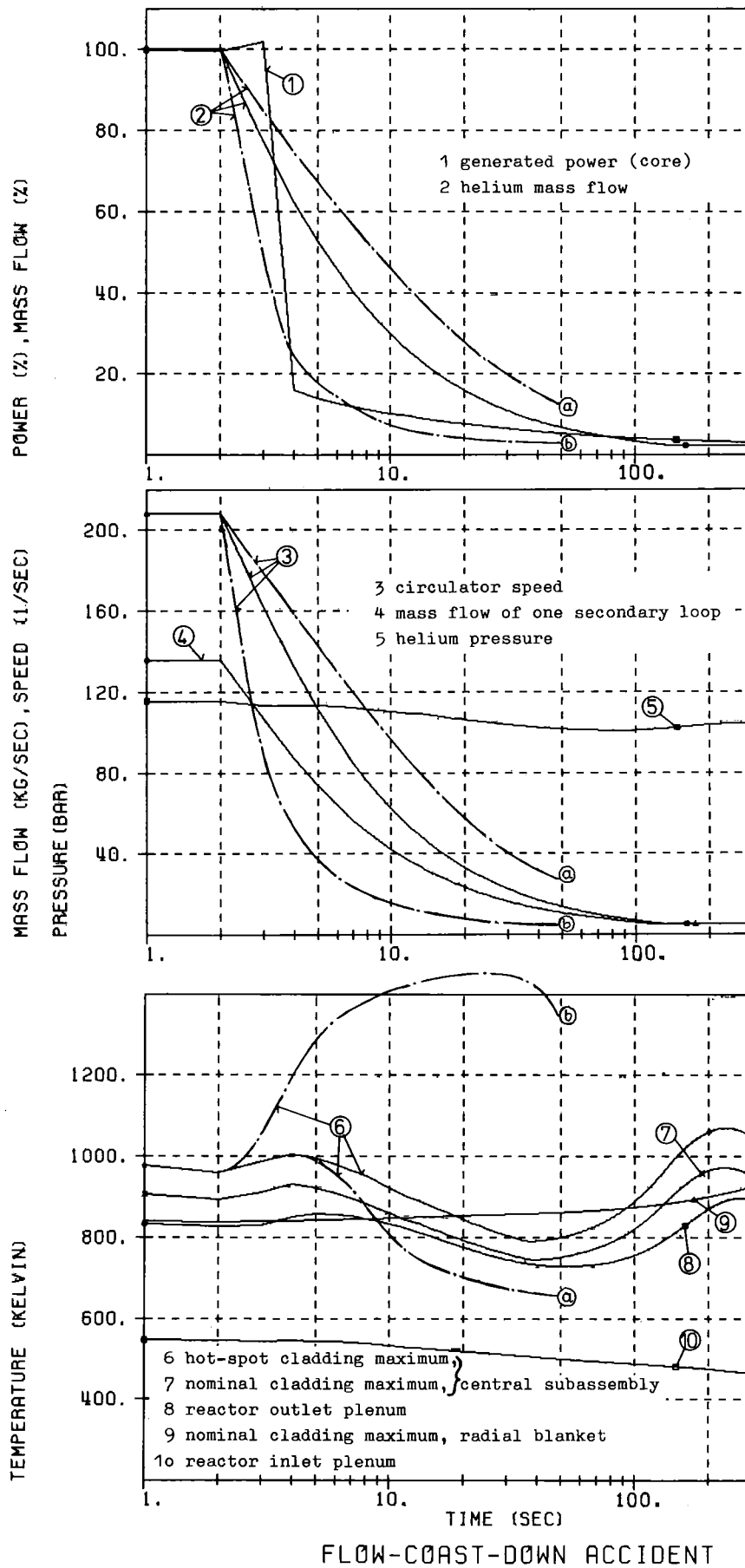
Fig.18 The main output of the first flow-coast-down accident

1 helium mass flow
2 mass flow of one secondary loop
3 feedback reactivity (no shut down rods)
4 generated power (core)
5 hot-spot cladding maximum, central subassembly
6 nominal cladding maximum, central subassembly
7 reactor outlet plenum
8 nominal cladding maximum, radial blanket
9 reactor inlet plenum

MASS FLOW (KG/SEC)

1600.

1200.

800.

400.

①
②

20.   40.   60.   80.   100.
TIME (SEC)

FLOW-COAST-DOWN ACCIDENT

POWER (%), REACTIVITY (CENT)

350.

300.

250.

200.

150.

100.

50.

③
④

20.   40.   60.   80.   100.
TIME (SEC)

TEMPERATURES (KELVIN)

4500.

4000.

3500.

3000.

2500.

2000.

1500.

1000.

500.

⑤
⑥
⑦
⑧
⑨

20.   40.   60.   80.   100.
TIME (SEC)
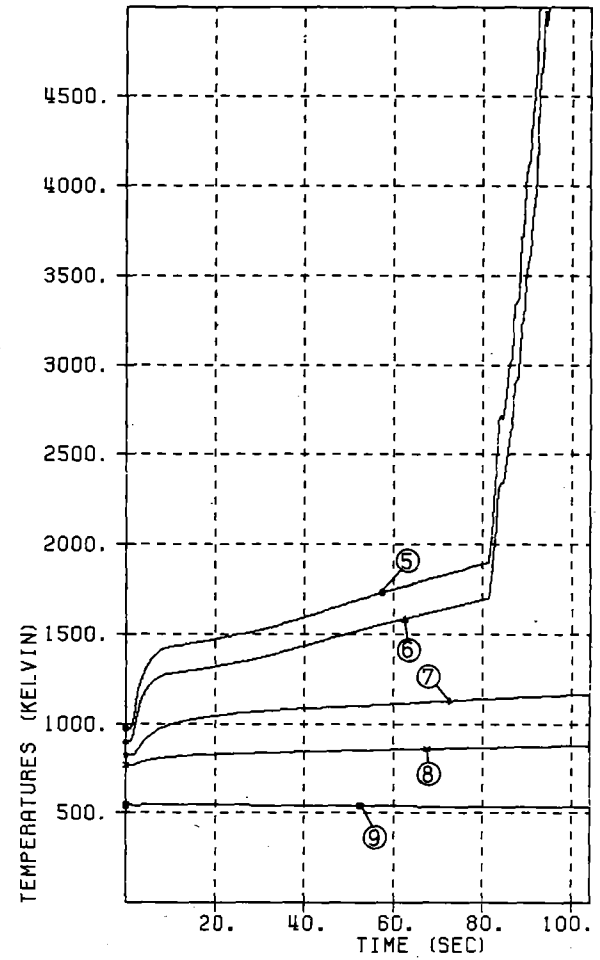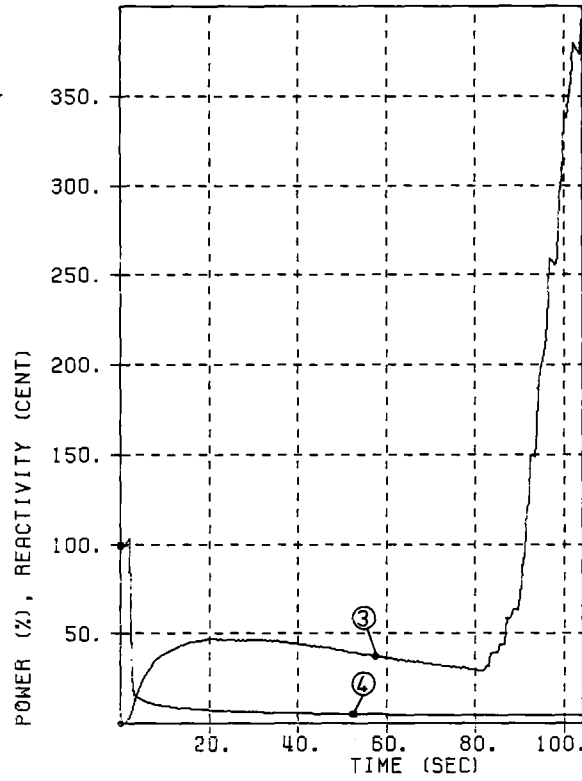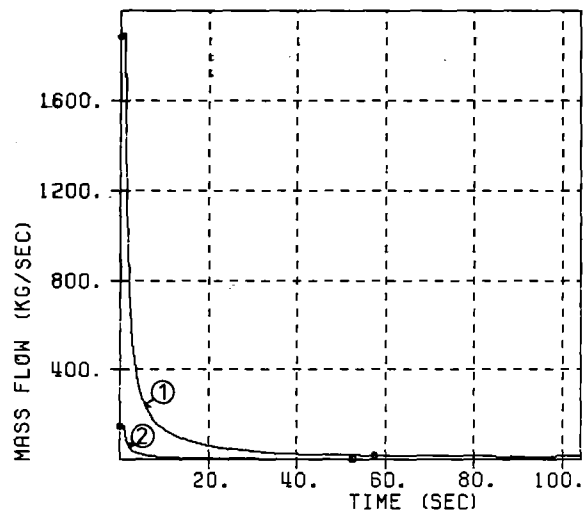
Fig.19   The main output of the second flow-coast-down accident

P1 - P7 Plenum of Helium Loop

1 Reactor Core
2 Resuperheater
3 Steam Generator
4 Helium Circulator
5 Node of Helium Loop

8 LOOPS

SCALE
1m
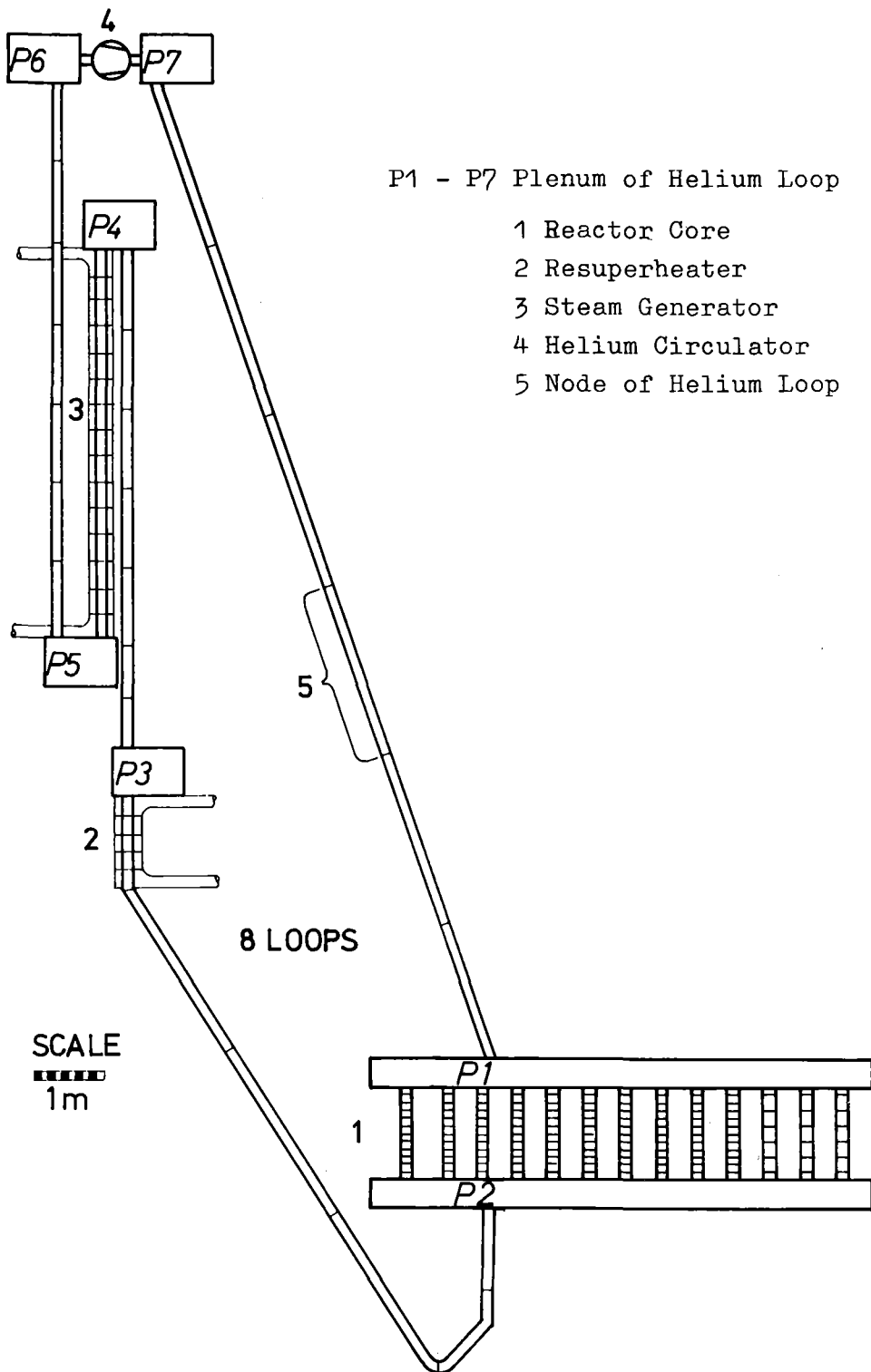
Fig.2o   PHAETON2-model of the 1ooo MWe reactor with
         13 core links and elevated steam generators

1 helium mass flow through the core
2 helium mass flow through the circulator
3 hot-spot cladding maximum, central subassembly
4 nominal cladding maximum, central subassembly
5 nominal cladding maximum, radial blanket
6 reactor outlet plenum
7 reactor inlet plenum
8 helium pressure
9 circulator speed
10 mass flow of one secondary loop
11 generated power (core)

FLOW-COAST-DOWN ACCIDENT

Fig.21 The main output of the third flow-coast-down accident